RNA (2001), *7*:1192–1212. Cambridge University Press. Printed in the USA.

DOI: 10.1017.S1355838201010330

Computational modeling of eukaryotic mRNA turnover

DAN CAO and ROY PARKER

Howard Hughes Medical Institute and Department of Molecular and Cellular Biology, University of Arizona, Tucson, Arizona 85721, USA

ABSTRACT

The process of eukaryotic gene expression involves a diverse number of steps including transcription, RNA processing, transport, translation, and mRNA turnover. A critical step in understanding this process will be the development of mathematical models that quantitatively describe and predict the behavior of this complex system. We have simulated eukaryotic mRNA turnover in a linear multicomponent model based on the known mRNA decay pathways in yeast. Using rate constants based on experimental data for the yeast unstable MFA2 and stable PGK1 transcripts, the computational modeling reproduces experimental observations after minor adjustments. Subsequent analysis and a series of *in silico* experiments led to several conclusions. First, we demonstrate that mRNA half-life as commonly measured underestimates the average life span of an mRNA. Second, due to the properties of the pathways, the measurement of a half-life can predominantly measure different steps in the decay network. A corollary of this fact is that different mRNAs will be affected differentially by changes in specific rate constants. Third, the way to obtain the largest change of levels of mRNA for the smallest changes in rate is by changing the rate of deadenylation, where a large amount of regulation of mRNA decay occurs. Fourth, the 3′-to-5′ degradation of mRNA shows mRNA-specific rates of degradation that are dependent on the 5′ structure of the mRNA. These programs can be run over the Web, are adaptable to other eukaryotes, and provide outputs as graphs and virtual northern gels, which can be directly compared to experimental data. Therefore, this model constitutes a useful tool for the quantitative analysis of the process and control of mRNA degradation in eukaryotic cells.

Keywords: degradation; eukaryotic; modeling; mRNA; multicomponent

INTRODUCTION

The process of eukaryotic gene expression involves a diverse number of steps that can be regulated in mRNA-specific manners. These steps include mRNA transcription, processing, transport, mRNP maturation, translation, and ultimately cytoplasmic mRNA turnover. To fully understand the regulation of mRNA biogenesis and function, it will be important to integrate our knowledge of the discrete steps in mRNA metabolism into a holistic understanding of the entire network. Such integration should be expected to reveal system properties and possible regulatory mechanisms that are a consequence of the integration of individual steps. One manner to begin integrating our understanding of mRNA metabolism is to develop mathematical models that quantitatively describe and predict the behavior of the process and regulation of mRNA biogenesis and function under a variety of circumstances. To develop such computational models, we have chosen to initially model the process of cytoplasmic mRNA turnover as related to overall mRNA metabolism for two reasons.

The first reason that cytoplasmic mRNA turnover is an ideal place to begin computational modeling of posttranscriptional gene expression is that the distinct steps in mRNA turnover pathways, and their temporal relationships, have been identified. Based on work primarily done in yeast, there appear to be two general pathways of mRNA degradation in eukaryotic cells (for review, see Beelman & Parker, 1995). In both general decay pathways, degradation of mRNA is initiated by the shortening of the poly(A) tail at the 3′ end. Shortening of the poly(A) tail to an A (oligo) length (deadenylation) leads to removal of the cap structure at the 5′ end (decapping), thereby exposing the transcripts to the digestion by a 5′-to-3′ exonuclease, which was blocked by the cap structure. Alternatively, the oligo (A) tail can be removed in a distinct process referred to as terminal deadenylation (Decker & Parker, 1993) and

Reprint requests to: Roy Parker, 1007 E. Lowell Street, Life Science South Building, University of Arizona, Tucson, Arizona 85721, USA; e-mail: rrparker@u.arizona.edu.

the body of the mRNA can subsequently be degraded in the 3′-to-5′ direction (Muhlrad et al., 1995). These appear to be the only two general pathways of decay, as yeast strains defective in both pathways are dead and show extremely long mRNA half-lives (Anderson & Parker, 1998). Understanding of this sequence of events provides critical information for the development of a mathematical framework for this process.

The second reason that cytoplasmic mRNA turnover is an ideal place to begin computational modeling is that a variety of rate constants have been measured for the distinct substeps in the turnover process. Two mRNAs that have been extensively studied in this regard are the yeast PGK1 mRNA, which is a relatively stable transcript ($t_{1/2} = \sim$30 min) and the MFA2 transcript, which is a relatively unstable mRNA ($t_{1/2} =$ 3–4 min). For both these mRNAs, the rates of deadenylation and decapping have all been measured experimentally (Muhlrad & Parker, 1992; Decker & Parker, 1993; Muhlrad et al., 1994, 1995). In addition, both of these mRNAs have been extensively analyzed with a poly(G) tract inserted into their 3′ UTRs. This poly(G) tract inhibits 5′-to-3′ and 3′-to-5′ exonucleases in vivo, and thereby allows the accumulation and detection of intermediates in the decay process. The analysis of the structure and abundance of these trapped decay intermediates has allowed the measurement of additional kinetic parameters. These include the rate of 3′-to-5′ exonucleolytic degradation and the rate of terminal deadenylation (Anderson & Parker, 1998; Schwartz & Parker, 2000). The measurement of these individual rates, or their estimation from experimental data, provides the quantitative information necessary for accurate simulation.

In this work, we have developed a computational model—CybermRNA1—for eukaryotic mRNA biogenesis and turnover, with a strong emphasis on the mRNA degradation steps based on the known pathways from yeast. The development of this model based on the existing literature allows us to examine our level of comprehension for the mRNA decay network. Importantly, our initial computational modeling reproduces experimental observations for the yeast unstable MFA2 and stable PGK1 transcripts with only minor deviations. This suggests that we have a relatively robust understanding for the steps of mRNA turnover. Such a model can then be used to rapidly examine *in silico* how the system responds to specific perturbations. Such *in silico* experiments can reveal new insights into experimental results and can identify cases where experimental results are inconsistent with the existing modeling results, thereby providing the basis for new mechanistic insights. As examples of this process, we have used this mathematical model to perform a series of *in silico* experiments on various decay steps that have led to new insights into the properties of the mRNA degradation network. In addition, we have written a Java applet to make this simulator run over the Web so it is accessible to anyone with a Web-connected computer. This model constitutes a useful, explanatory tool to allow a quantitative analysis for the pathways involved in mRNA degradation.

RESULTS

The biological and mathematical model

The pathways

In this work, we constructed the mathematical framework shown in Figure 1. The process starts with transcription of the mRNA (k1), which we assume is a zeroth-order process. Transcription produces a pool of nuclear mRNA, which can be considered analogous to hnRNA. We have not modeled the diversity of RNA processing events that can occur within the nucleus, although we have included a pathway for nuclear decay because there is evidence that mRNAs may be degraded in the nucleus (Bousquet-Antonelli et al., 2000). However, because there is limited kinetic information about the rate or amount of nuclear decay, we have kept the rate constant for this step (k6) at zero in our initial simulations presented here. In the second step, the mRNA is transported to the cytoplasm (k2). mRNAs can then either enter poly(A) shortening or be subjected to deadenylation-independent decapping (k7). Deadenylation-independent decapping occurs in a process referred to as mRNA surveillance wherein aberrant mRNAs, such as those containing premature termination codons, are rapidly degraded (for review, see Hilleren & Parker, 1999). In our initial modeling of normal mRNAs, we have kept the rate of deadenylation independent decapping at zero, because no normal transcript is expected to enter this branch, and modeling of this pathway of mRNA degradation will be presented elsewhere.

The remainder of the major pathway is modeled as follows. To simulate the poly(A) shortening process, we assume all transcripts start with a poly(A) tail length of 70 (Decker & Parker, 1993). This is a minor simplification of the observed situation where the initial poly(A) tail length may vary by $\leq$10 nt between different mRNAs (Brown & Sachs, 1998). The poly(A) tails are then shortened first through an initial deadenylation phase (70A–60A, r1) that is slower than the subsequent poly(A) shortening process (see Decker & Parker, 1993), which we have modeled in 5 equally divided phases during which the rate remains constant (r2–r6): 60A–50A, 50A–40A, 40A–30A, 30A–20A, 20A–10A. Once the mRNA reaches an oligo (A) length of approximately 10–12 residues, it can be a substrate for a decapping reaction (k3), followed by 5′-to-3′ exonucleolytic degradation (k4). This produces an mRNA fragment trimmed to the 5′ side of the poly(G) tract, referred to as the 3′ mRNA

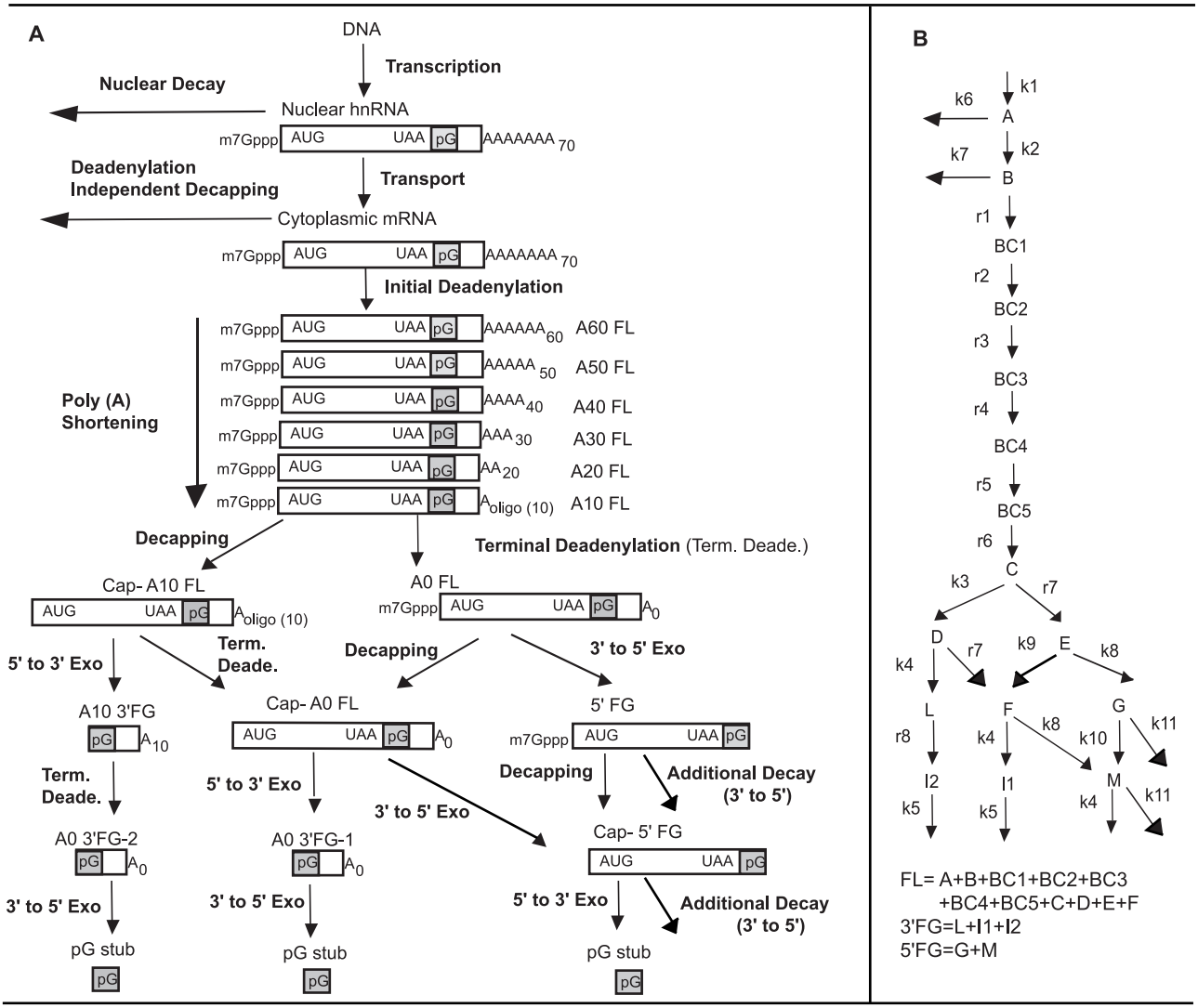

FIGURE 1. Schematic representations for the linear multicomponent model. **A:** The concrete conceptual model. **B:** The symbolized model. The symbols are used in the math equations and computer program for corresponding component and kinetic parameter. All of the full-length (FL) species (A, B, C, D, E, F, BC1–BC5) are summed to report the full-length half-life, average life span, and total full-length transcript level; L, I1, and I2 are summed as 3′ fragment (3′ FG). G and M are summed as 5′ fragment (5′FG). (The same abbreviations are used throughout this article.)

fragment (Decker & Parker, 1993; Muhlrad et al., 1994, 1995). This mRNA fragment then undergoes further deadenylation from 10A to 0A (r8), referred to as terminal deadenylation (Decker & Parker, 1993), and becomes a substrate for 3′-to-5′ exonucleolytic degradation, producing a small segment corresponding to the poly(G) tract, referred to as the poly(G) stub (Anderson & Parker, 1998).

A branch point in the model occurs when mRNAs reach an oligoadenylated species. Here the full-length mRNA can also undergo terminal deadenylation (r7), prior to decapping of a fully deadenylated species (k9), which also produces an mRNA 3′ fragment by 5′-to-3′ exonucleolytic digestion of the full-length mRNA (k4). Alternatively, the A0 full-length mRNA can also be a substrate for 3′-to-5′ exonucleolytic degradation (k8; Anderson & Parker, 1998), which produces a 5′ mRNA fragment trimmed to the 3′ side of the poly(G) tract. This 5′ mRNA fragment is then subjected to decapping (k10) and 5′-to-3′ exonuclease digestion (k4), as well as continued degradation by an unknown mechanism, which is likely to be additional 3′-to-5′ degradation (k11). We have added this additional step (k11) because the 5′ fragment shows a half-life of ~30 min in a dcp1Δ strain (Anderson & Parker, 1998 and unpubl. observations), where all decapping is blocked (Beelman et al., 1996). This suggests that there is an additional mechanism by which this 5′ mRNA fragment can be degraded. We found if we use the same value for this step as the 3′-to-5′ decay rate (k8), the simulated results match well with the experimental observations seen in dcp1Δ strains.

Simplifications and assumptions

There are several assumptions in the above mathematical framework we build. First, we assume transcription is a zeroth-order process and all the other decay steps are first-order processes, which might not necessarily be true. Second, we assume all the steps are irreversible, which might not be true for all cells. For example, in some cases, cytoplasmic readenylation can occur (for review, see Gray & Wickens, 1998). Third, we assume there is no coupling between steps in either a forward direction or through positive or negative feedback, which might not be true under some circumstances (e.g., Hilleren & Parker, 2001). We make these simplifications and assumptions to begin developing the mathematical model. Specific discrepancies found between modeling results and experimental results might invalidate some of the original assumptions, and suggest the existence of previous unknown pathways or mechanisms. This notice of discrepancies and modification of the model to more accurately reflect the experimental results might lead to new insights. However, our ability to reasonably mimic in vivo results with our current model suggests that, at least to the first approximation, our assumptions are reasonable.

The programs

In our programs, we described the amount of each species in the mRNA decay network by a series of differential equations (see Methods). Based on these equations, we modeled two types of situations. First, we modeled the results of decay from a steady-state condition. This is analogous to the most common method of measuring mRNA decay rates wherein transcription is inhibited either by conditional mutants or by drugs, and the loss of a particular mRNA is then followed over time (for methods, see Parker et al., 1991). In this case, every component starts from its steady-state level at time 0, when transcription rate (k1) is set to zero, and the changes in the amount of each species are followed over time. This program also calculates the expected amount of each species in the network under steady-state conditions.

We also modeled a "transcriptional pulse-chase" experiment. In this procedure, a regulatable promoter is used to induce a pulse of transcripts that are synthesized within a short period, which are then followed during a subsequent chase period where transcription is inhibited (e.g., Shyu et al., 1991; Decker & Parker, 1993). To simulate the transcriptional pulse-chase experiment, every component starts from an initial amount of zero, transcription is induced *in silico* for 2 min, and then the transcription rate is set to zero. In actual pulse-chase experiments with yeast cells, the transcription induction is usually 5–10 min (Decker & Parker, 1993). We utilized a shorter "pulse" time *in silico* because in the computer program, transcription is idealized at an equal rate upon the start. In contrast, there is a lag in response to the inducible promoter before transcription is fully induced in real experiments (C.J. Decker & R. Parker, unpubl observations).

In each of these programs, the amount of each component is computed every second and output in the form of a graph that can show the amount of every component as a function of time. The programs also provide an output as a simulated northern gel comparable to what would be seen from a real experiment. To do this, we take the amount of every component at various time points and draw a rectangle with the gray scale corresponding to the amounts of the particular mRNA species that migrate together on the high-resolution northern gel (e.g., species with the same poly(A) tail range and species with or without the cap structure). Mapping the quantitative value to 256 different gray scale levels does the conversion. This allows simple and direct comparison of actual and simulated experiments.

The programs also calculate two values. In the decay from steady-state program, the half-life is calculated as is traditionally done as the point at which the amount of the full-length mRNA reaches half of the initial value. In the pulse-chase program, the average life span is calculated, which is the time for the mRNA produced during the brief pulse to reach half its value at the end of the pulse. This value is a measurement of how long a given mRNA molecule persists in the cell. All of these programs are coded as Java 1.1 applet, which is a Web-based program and can be used by anyone with an Internet-connected computer using Internet Explorer version 4 or higher. The running time is less than 1 min with a regular PC or Mac and the programs can be accessed through http://www.mcb.arizona.edu/Parker/default.html.

Modeling of the degradation of the MFA2pG and PGK1pG mRNAs

To determine how well these programs reproduce the in vivo decay network, we modeled the metabolism of two yeast mRNAs. In this modeling, we utilized the MFA2pG and PGK1pG mRNAs for three reasons. First, they represent a stable and an unstable mRNA in yeast, although they both are predominantly degraded at 5′-to-3′ direction. Second, their degradation has been extensively characterized and there is a wealth of kinetic data that allows us to accurately assess, or at least estimate, the rate constants for the individual steps in the model. Third, they have been studied under conditions where the poly(G) tract in their 3′ UTRs has allowed the levels of decay intermediates to be assessed, which is a useful readout of the process in vivo. The rate constants we utilized for modeling the decay of the MFA2pG and PGK1pG transcripts (shown in Table 1) are based on either direct measurement of various rates

TABLE 1. Kinetic parameters (as unit/second or s^{-1}) used in the modeling for MFA2pG and PGK1pG.

Kinetic parameter and event/reaction		MFA2pG	PGK1pG	Logic
k1	Transcription	1	1	Does not matter, arbitrary value
k2	Transport	0.2	0.2	Adjust at the end to give 1–2% nuclear distribution for MFA2
k3	Decapping for A oligo	0.0077	0.000462	From $t_{1/2}$ of A oligo in pulse-chase exp.
k4	5′ → 3′ exonuclease	1	1	Arbitrary set for fast rate because of very low level of cap-intermediates
k5	3′ → 5′ decay for fragment	0.0009	0.001	Adjust to give the correct fragment $t_{1/2}$
k6	Nuclear decay	0	0	Little information, set to zero
k7	Deadenylation-independent decapping	0	0	Normal transcripts are not expected to enter this branch
k8	3′ → 5′ decay for full length	0.0012	0.0003	Adjust to fit with the observed mRNA $t_{1/2}$ when decapping is blocked
k9	Decapping for A0	0.0077	0.000462	Assume the same as k3
k10	Decapping for 5′ fragment	0.077[a]	0.00462[a]	Adjust later to fit with the observed 5′ fragment level
k11	Additional decay for 5′ fragment	0.001201	0.00031	Add later to fit with the observed 5′ fragment $t_{1/2}$
r1	Full-length 70A–60A	0.011	0.0042	Measured from pulse-chase gel ($cr_1 - r_6$). Calculated as the reciprocal of time (s) to complete poly(A) shortening within the 10 A range
r2	Full-length 60A–50A	0.022201	0.0040	
r3	Full-length 50A–40A	0.022202	0.0038	
r4	Full-length 40A–30A	0.022203	0.0036	
r5	Full-length 30A–20A	0.022204	0.0034	
r6	Full-length 20A–10A	0.023	0.0032	
r7	Full-length 10A–0A	0.00222	0.00111	Assume same as r8
r8	3′ Fragment 10A–0A	0.0022201	0.0011	Measured from pulse-chase gel
pG	efficiency for 5′ → 3′ exonuclease	0.3[a]	0.8[a]	Adjust later to fit with the observed 3′ fragment level
pG	efficiency for 3′ → 5′ exonuclease	0.3[a]	0.5[a]	Adjust later to fit with the observed 5′ fragment level in either wild type (PGK1) or decapping mutant (MFA2)

[a]Adjusted from the initial value according to the logic stated in the results.

in wild-type or mutant strains, or inferred from steady-state ratios of critical decay intermediates. (For more discussion of the derivation of the rate constants and implicit assumptions, see the Methods section.)

MFA2pG

Using the rate constants for the MFA2pG mRNA (Table 1), we generated modeling results using the decay from the steady-state program and the pulse-chase program (Fig. 2A). This can be compared to actual experimental data (Fig. 2B). In general, the behavior of the *in silico* system accurately reproduces the experimental observation in terms of half-life and the steady-state poly(A) distribution of the full-length mRNAs. For example, the predicted $t_{1/2}$ of the MFA2 transcript is 3.8 min and the measured $t_{1/2}$ is between 3 and 4 min. However, we observed that our simulations led to an overabundance of mRNA 3′ fragment generated by 5′-to-3′ exonucleolytic degradation. For example, the simulation gives us a 1-to-3 ratio of full-length mRNA to 3′ fragment at steady state (table in Fig. 2), whereas the actual observed ratio is roughly 1 to 1 (Hatfield et al., 1996). Similarly, in the real pulse-chase experiment, the levels of mRNA fragment peak at 30% of the initial full-length mRNA levels, whereas *in silico*, the amount of fragment peaks at ~80% of the maximum full-length level (compare Fig. 2A and B).

In principle, there are several possible explanations for the overabundance of the mRNA fragment in our simulation experiment. First, it could be that we have underestimated the rate of terminal deadenylation and 3′-to-5′ decay of the fragment. However, this is unlikely, as our *in silico* fragment half-life (14.9 min) was quite close to experimental data (15 min; Anderson & Parker, 1998). Another possibility is that we overestimated the amount of mRNA that is decapping and degraded to produce fragment, and that a substantial amount of the full-length mRNA is degraded by a different, and as yet unknown, decay mechanism. However, this is unlikely because lesions that block mRNA decapping or 5′-to-3′ exonuclease digestion lead to a substantial stabilization of the majority of the full-length mRNA in transcription pulse-chase experiments (Muhlrad et al., 1994; Beelman et al., 1996; Dunckley & Parker, 1999). A simple explanation for the overabundance of mRNA fragment *in silico* is that the poly(G) structure is not a

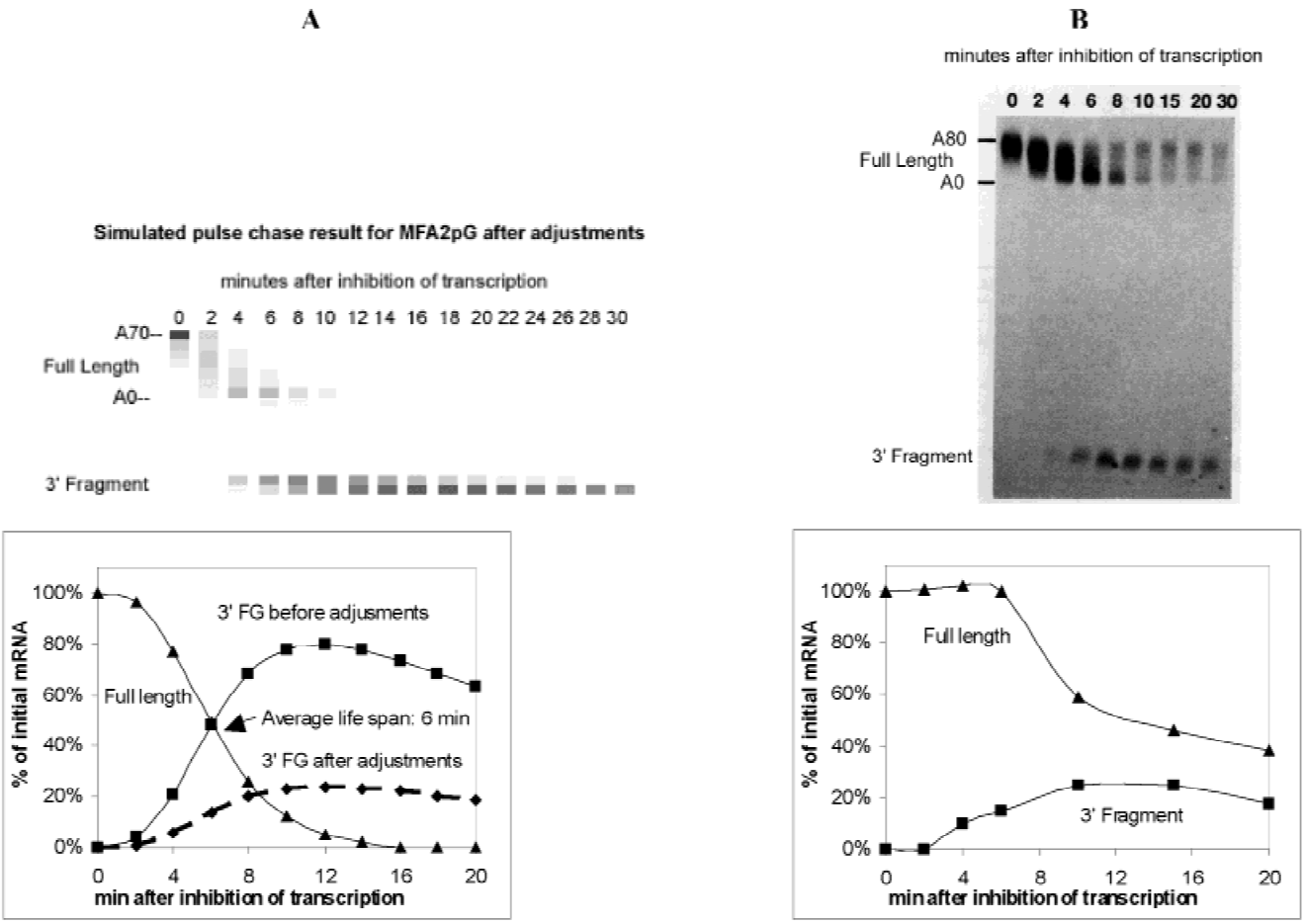

	$T_{1/2}$(Min)	Full-length	3′ fragment	5′ fragment
Computed before adjustments	3.8	24%	76%	~0
Computed after adjustments	3.8	51%	49%	~0
Actual observed	3-4	53%[1]	47%[1]	~0

[1]From Anderson and Parker, 1998.

FIGURE 2. Comparison of simulated results and actual experimental results for MFA2pG. The correspondent kinetic parameters used are listed in Table 1. **A:** The computed results. **B:** The observed experimental pulse-chase result (Decker & Parker, 1993). The points represent the mean of three separate experiments. The increase in RNA levels seen during early time points is most likely due to incomplete repression of transcription, which probably also contributes to other differences from simulation in **A**. In the simulation, if we keep a 10% residual transcription after the 2 min "pulse," we can reproduce the graph shown in **B**.

100% effective block to the 5′-to-3′ exonuclease. Several lines of experimental evidence support this latter possibility. First, when mRNAs contain multiple poly(G) tracts, mRNAs fragments are observed where the 5′-to-3′ exonuclease stalls at the 5′ end of each poly(G) tract (Vreken & Raue, 1992; Muhlrad et al., 1994). This argues that the exonuclease can sometimes digest through the poly(G) tract, possibly because the poly(G) structure does not always fold into the most stable secondary structure. Second, if the poly(G) tract is a complete block to exonucleases, we would expect the summation of full-length, mRNA fragment and poly(G) stub should remain constant after transcription is turned off. In addition, we should see a significant amount of poly(G) stub appearing when both the full-length and fragment are disappearing in the decay from steady-state and pulse-chase experiments. In fact, very low levels of the poly(G) stub are observed (Anderson & Parker, 1998). Based on the above arguments, we conclude that the poly(G) tract is not a complete block to the 5′-to-3′ exonuclease. Given this, we added a poly(G) efficiency factor into the model, which reflects the percentage of the time that the poly(G) tract inhibits the progression of the 5′-to-3′ exonuclease. If the poly(G) tract in the MFA2pG mRNA is set to block the 5′-to-3′ exonuclease at 30% efficiency, the simulated levels of 3′ fragment closely match the experimental results in both steady-state distribution and in the pulse-chase program (compare Fig. 2A and B, Fig. 2 table). Values that are lower than 30% give a lower simulated 3′ frag-

ment level than observed, and values that are higher than 30% give a higher simulated 3′ fragment level than observed. Therefore, the poly(G) efficiency of 30% is solely based on *in silico* calculations. Thus, after this adjustment, the behavior of the MFA2pG mRNA *in silico* is similar to the observed experimental situation.

PGK1pG

The initial results for the modeling of the PGK1pG mRNA also closely reproduced the experimental observation (e.g., predicted $t_{1/2}$ = 27 min, observed $t_{1/2}$ ~ 30 min). However, the modeling of PGK1pG also generated more 3′ mRNA fragment than observed (Fig. 3). Based on our prior examination of the MFA2pG mRNA, we hypothesized that this discrepancy would again be due to the poly(G) tract not being an absolute block to the 5′-to-3′ exonuclease. In this case, *in silico* experiments indicated that if the poly(G) works at 80% efficiency for PGK1pG mRNA, the simulated amount of 3′ fragment closely matches experimental observations. It is not unreasonable for different poly(G) tracts to have different effectiveness because we know the exonuclease stalls at different positions relative to the poly(G) tract in different mRNAs (cf. Decker & Parker, 1993; Muhlrad et al., 1994, 1995). This suggests that the local sequence context can influence the structure formed by the poly(G) tract or the probability of poly(G) tract folding into the appropriate structure, and therefore presumably its ability to inhibit exonucleases.

The modeling of PGK1pG also predicts higher levels of the 5′ mRNA fragment produced from 3′-to-5′ decay

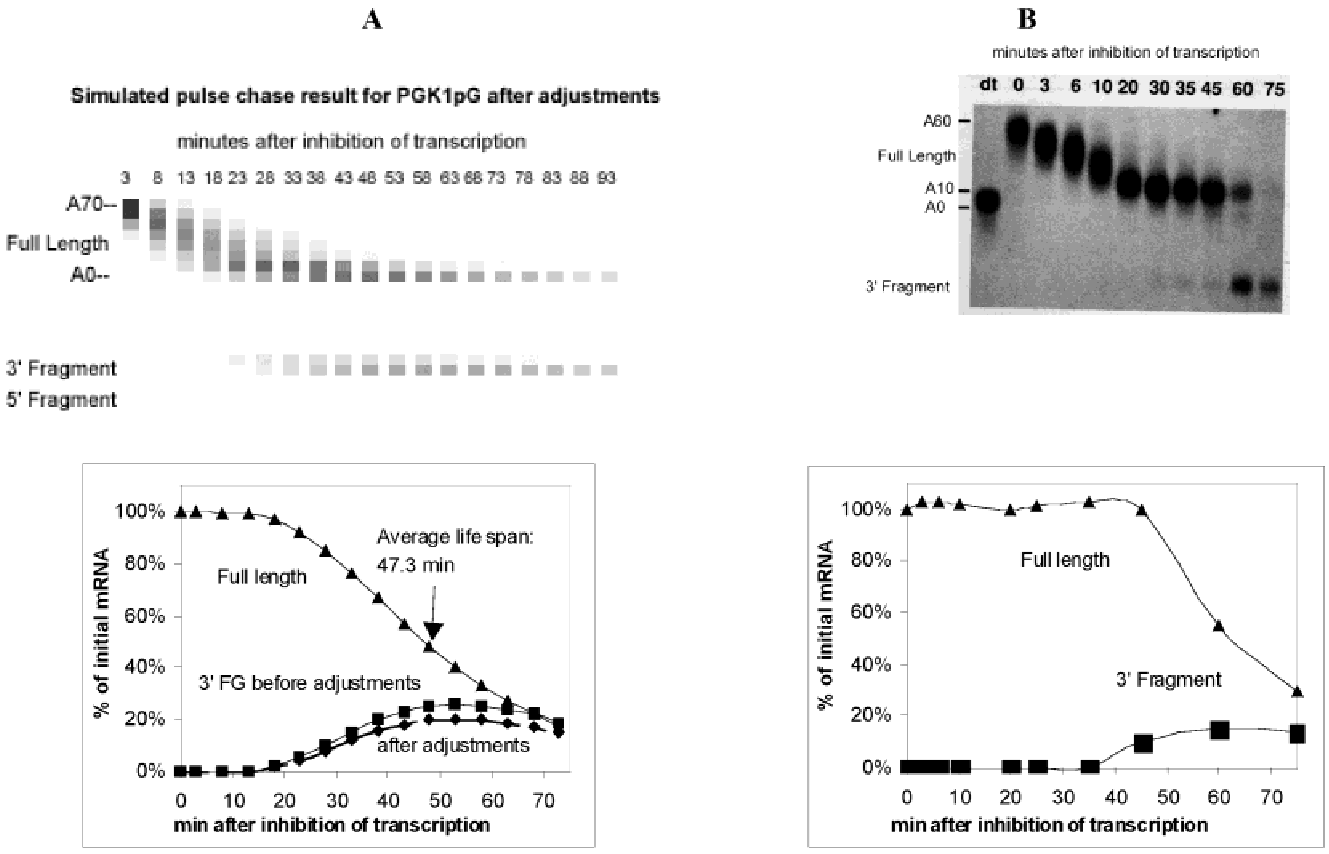

	$T_{1/2}$(Min)	*Full-length*	*3′ fragment*	*5′ fragment*
Computed before adjustments	27.4	71%	22%	36% of 3′ fragment
Computed after adjustments	27.4	80%	19%	4% of 3′ fragment
Actual observed	~30	79%[1]	21%[1]	5% of 3′ fragment[2]

[1]From Anderson and Parker, 1998.
[2]From Mulhrad et al., 1995.

FIGURE 3. Comparison of simulated results and actual experimental results for PGK1pG. The correspondent kinetic parameters used are listed in Table 1. **A:** The computed results. **B:** The observed experimental pulse-chase result (Decker & Parker, 1993). The increase in RNA levels seen during early time points is most likely due to incomplete repression of transcription, which probably also contributes to other difference from the simulation in **A**. In the simulation, if we keep a 1% residual transcription after the 2 min "pulse," we can reproduce the graph shown in **B**.

than are actually observed experimentally. Specifically, this 5′ mRNA fragment is present at ~40% of the levels of the 3′ mRNA fragment at steady state in the initial modeling (Fig. 3). However, the 5′ fragment is estimated to be present at only ~5% of the level of the 3′ fragment by experimentation (Muhlrad et al., 1995). There are three possible reasons for this disparity. First, it could be that the rate of 3′-to-5′ decay is overestimated in our simulations due to overestimates of the rates of either terminal deadenylation or 3′-to-5′ degradation. This possibility is unlikely because the predicted half-life (51 min) using this combination of rate constants when the decapping rate is set to 0 is quite close to what is measured in strains unable to perform decapping, wherein all mRNA decay occurs by 3′-to-5′ degradation ($t_{1/2}$ measured in dcp1Δ strains is 45 ± 5 min; Beelman et al., 1996). Second, it is possible that the decapping rate of the 5′ fragment is underestimated. This is a reasonable assumption, as it is known that there is extensive communication between the 5′ and 3′ ends of the mRNA and that features of the 3′ end of the mRNA can affect the rate of decapping (e.g., Muhlrad et al., 1994; Muhlrad & Parker, 1999). Given this, we assigned a decapping rate for the 3′ trimmed mRNAs (5′ fragment) to be 10 times faster than the decapping rate of the oligoadenylated full-length species. Finally, it is also likely that the poly(G) is not a complete block to 3′-to-5′ decay. If we assume the poly(G) tract functions at similar efficiency for both 5′-to-3′ decay (80%) and 3′-to-5′ decay (50%), we obtain modeling results that are quite consistent with experimental observations (cf. Fig. 3A and B).

There are other possible manners to resolve the excess of predicted mRNA fragment. We do not exclude the existence of other reasonable possible ways to solve this discrepancy. For example, the poly(G) might be a very poor block to 3′-to-5′ decay (5%) and the decapping rate for the 5′ fragment is the same as that for the oligoadenylated full-length mRNA. Alternatively, the decapping rate for 5′ fragment could be 20-fold faster than that of oligoadenylated full-length mRNAs and the poly(G) serves as a complete block to 3′-to-5′ decay. However, we think that the adjustments to make the 5′ fragment have a 10-fold faster decapping rate and the poly(G) tract is a partial block to 3′-to-5′ decay is simplest and quite reasonable. Therefore, we used this combination of adjustments for all of our subsequent analysis. We also adjusted the poly(G) efficiency for 3′-to-5′ decay (30%) and decapping rate for 5′ fragment similarly for MFA2pG for two reasons. First, the simulation of MFA2pG when decapping is blocked also leads to an overabundance of 5′ mRNA fragment compared to observed experimental data (Beelman et al., 1996; Anderson & Parker, 1998), although the simulated 5′ fragment level seems to fit well with the observed level under the wild-type condition. Second, the generality of these pathways suggests that MFA2pG and PGK1pG may be subject to the same type of parameters.

Effects of changes in rate constants on mRNA levels, decay rate, and other parameters

The results above demonstrate that following minor reasonable adjustments, we were able to closely reproduce the in vivo mRNA turnover process with *in silico* simulations. Given this fact, these simulations are useful tools for examining the properties of the mRNA decay network. We have used the kinetic models described above to examine how the behavior of the MFA2pG and PGK1pG mRNAs changes in response to alteration in various rate constants. These *in silico* experiments are analogous to two types of biological situations. First, a change in a specific rate constant could be due to a lesion that alters that process. For example, deletion of the DCP1 gene, which encodes the decapping enzyme, leads to what appears to be an absolute block to decapping (Beelman et al., 1996). Such a situation can be modeled by setting the rate constants for decapping steps to zero. Alternatively, deletion of a variety of general decapping activator proteins lead to partial defects in the rate of decapping, which can be simulated by more modest changes in the rate constants for decapping (Boeck et al., 1998; Tharun et al., 2000). These *in silico* experiments also model the changes in a specific rate that might occur in response to a particular biological stimulus, or the loss of a key regulatory protein. The results of how changes in specific rate constants affect mRNA metabolism by a number of criteria have been examined for transport, deadenylation, decapping, 3′-to-5′ exonucleolytic decay, and 5′-to-3′ exonucleolytic decay.

Changes in mRNA transport

The results of changes in the rate of mRNA transport are shown in Table 2. Several points can be made from this simulation. First, severe changes in transport rate have little effect on the overall system as assessed by decay rates and steady-state mRNA levels. For example, a 100-fold decrease in the rate of transport leads only to a 2.1-fold increase in the half-life for the MFA2pG mRNA and only a 1.1-fold increase in the half-life for the PGK1pG mRNA. The minimal effect of changes in the rate of transport can be understood as a simple consequence of this step being significantly faster than steps in cytoplasmic decay. An obvious limitation of this analysis is that there is very little experimental data to derive a rate constant for the actual rate of mRNA transport. Therefore, our initial estimation of the rate constant for transport could be too fast, which might change the quantitative, but not qualitative, nature of this result.

TABLE 2. MFA2pG and PGK1pG *in silico* transport mutants.

	Wild type (WT)		10× WT		1/10 WT		1/100 WT		1/1,000 WT	
Category	MFA2	PGK1	MFA2	PGK1	MFA2	PGK1	MFA2	PGK1	MFA2	PGK1
Transport rate (k2)	0.2	0.2	2	2	0.02	0.02	0.002	0.002	0.0002	0.0002
Half-life (min)	3.8	27.4	3.8	27.4	4.1	27.8	8.1	31.4	58.1	72.8
Life span (min)	6	47.3	5.9	47.2	6.5	48.0	12.6	55.8	64.2	113.1
Full length	446	3206	442	3201	491	3251	941	3701	5441	8201
HnRNA	5	5	0.5	0.5	50	50	500	500	5000	5000
Nuclear %	1.12%	0.2%	0.11%	0.02%	10%	1.5%	53%	13.5%	91.9%	61%

A second important point is that decreases in transport rate, although not affecting mRNA decay substantially, do lead to a more dramatic increase in the pool of nuclear mRNA (Fig. 4). For example, a 100-fold decrease in the rate of transport led to the presence of 13.5% and 53% of the PGK1 and MFA2 transcripts, respectively, in the nucleus. This provides a satisfactory explanation for why many mRNA export mutants, which were isolated based on the accumulation of poly A+ RNA in the nucleus, show little effect on the metabolism of individual mRNAs (Neville & Rosbash, 1999; Hilleren & Parker, 2001).

Changes in mRNA deadenylation

Several points can be made from simulations examining alterations in the rates of mRNA deadenylation (Table 3). In this set of simulations, we varied the rates of all the steps in deadenylation, including terminal deadenylation, by the same magnitude. First, changes in deadenylation rate lead to changes in mRNA levels, half-life, and average life span. As compared to changes in other steps in the decay pathway, the alterations in deadenylation rate lead to the largest changes in mRNA metabolism (see comparison in Fig. 5). This can be understood in that deadenylation is a requisite step for both downstream decay pathways. The relationship between deadenylation rate change and mRNA half-life is shown in Figure 5.

A second interesting point is that changes in overall deadenylation rate do not have much effect on the poly(A) distribution of full-length mRNA species at steady state, except for the amount of the A-oligo and A0 (Table 3, Fig. 6A–C). This is true as long as all the steps in the deadenylation pathway are affected the same magnitude. For example, when the deadenylation rate decreases, all of the A70–A20 species increase by the same fold. The A10 and A0 species do not increase as much, because they are still subject to decapping, whose rates still remain unchanged. Therefore, when the deadenylation rate decreases, we see a loss of the oligoadenylated and A0 species with the remainder of the

TABLE 3. MFA2pG and PGK1pG *in silico* deadenylation mutants.[a]

	Wild type (WT)		5× WT		10× WT		1/5 WT		1/10 WT	
Category	MFA2	PGK1	MFA2	PGK1	MFA2	PGK1	MFA2	PGK1	MFA2	PGK1
Half-life (min)	3.8	27.4	1.7	16.2	1.4	15.5	14.4	85.0	27.8	155
Life span (min)	6	47.3	1.9	21.0	1.5	17.6	26.2	159.1	49.8	290
Full length	446	3206	188	1711	154	1516	1708	10073	3281	18363
5′ Fragment	0.1	28	0.3	37	0.4	38	0.03	13	0.02	8
3′ Fragment	428	791	318	520	303	500	969	3139	1645	6560
Cyto A70 FL[b]	91	238	18	48	9.1	29	455	1190	909	2381
A60 FL	45	250	9	50	4.5	25	225	1250	450	2500
A50 FL	45	263	9	53	4.5	26	225	1316	450	2632
A40 FL	45	278	9	56	4.5	28	225	1389	450	2778
A30 FL	45	294	9	59	4.5	29	225	1471	450	2941
A20 FL	43	313	9	63	4.3	31	217	1562	435	3125
A10 FL	101	640	53	168	33	87	123	1466	126	1748
A0 FL	25	924	66	1211	83	1259	6	423	3	252
A10 3′ FG	105	213	11	11	3	3	639	2441	1313	5821
A0 3′ FG[c]	323	578	307	509	299	497	331	698	332	739

[a] r1–r8 are changed by equal magnitude in all mutants.
[b] This does not include the 5 units of HnRNA that we assume also has an A tail length of 70. This is the same for all other tables.
[c] This is the summation of A0 FG-1 and A0 FG-2. This is the same for all other tables.

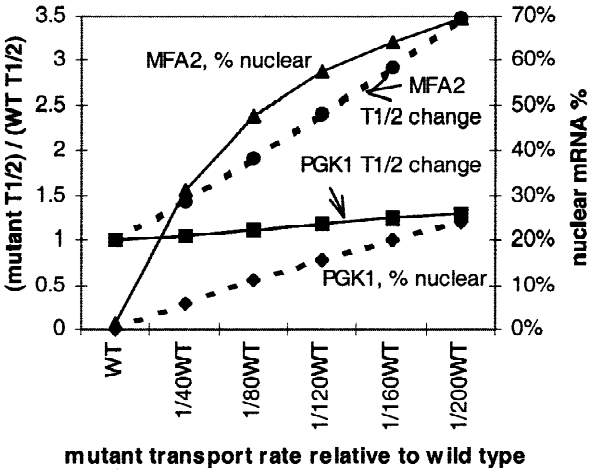

FIGURE 4. Effects of MFA2pG and PGK1pG *in silico* transport mutants on half-life change and relative nuclear transcript level.

distribution not changing substantially. Similarly, when the deadenylation rate increases, we can see an accumulation of the oligo and A0 in the poly(A) distribution because the decapping rate remains the same for A10 and A0 species. A corollary of this fact is that conditions that alter the poly(A) distribution (A70–A20) of an mRNA must either differentially affect different steps in the deadenylation phases (e.g., see Tucker et al., 2001), or must affect additional steps downstream of deadenylation such as decapping (see Muhlrad et al., 1995; Olivas & Parker, 2000).

Changes in mRNA decapping

The results of changes in the rate of mRNA decapping are shown in Table 4. Several points can be made from this simulation. First, although changes in decapping rate affect mRNA decay rates, the magnitude of the effect is smaller than what is observed with similar changes in deadenylation rates (see Fig. 5 for comparison). For example, a 10-fold decrease in the rate of decapping leads to 2.4-fold stabilization of the MFA2pG mRNA, whereas this change in the rate of deadenylation led to a 7.4-fold increase in the predicted $t_{1/2}$. This difference can be understood as a consequence of the fact that deadenylation is a prerequisite for all decay, whereas in the absence of decapping, degradation can still occur by a 3′-to-5′ exonucleolytic mechanism.

A second important point is that the MFA2pG mRNA is more responsive to decreases in decapping rate than the PGK1pG mRNA. For example, whereas a 10-fold decrease in decapping rate stabilizes the MFA2 mRNA 2.4-fold, this change in decapping only stabilizes the PGK1pG mRNA 1.7-fold. This difference can be attrib-

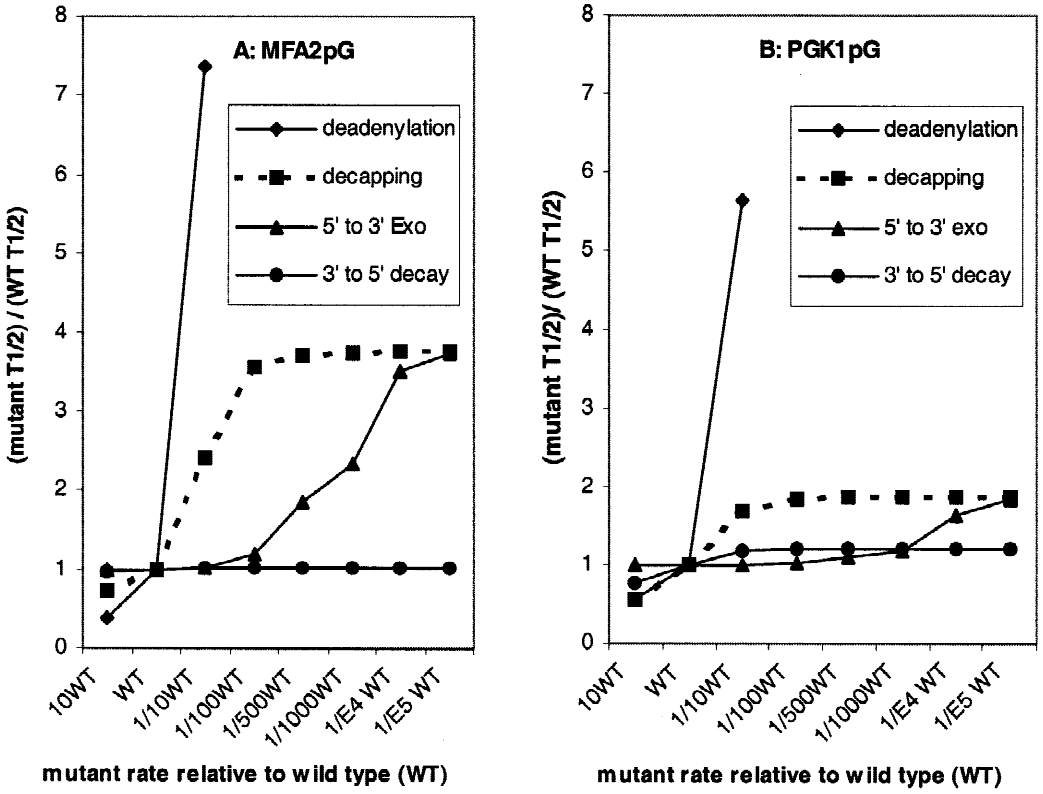

FIGURE 5. Comparison of *in silico* deadenylation, decapping, 5′-to-3′ exonuclease, and 3′-to-5′ decay mutants. **A:** MFA2pG. **B:** PGK1pG.

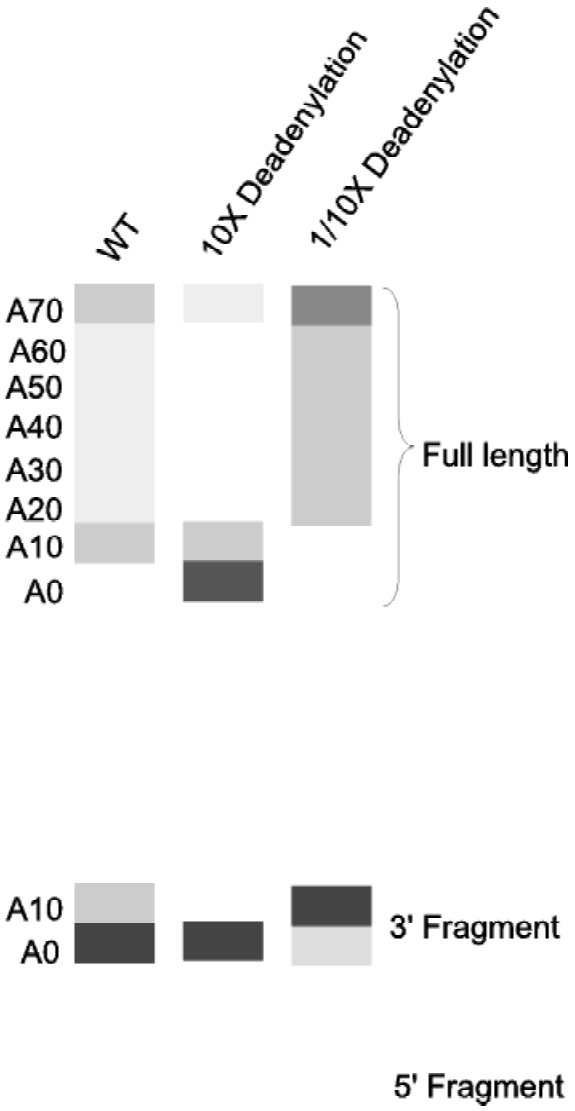

FIGURE 6. Computed steady-state poly(A) distribution of MFA2pG wild type (WT), a mutant whose deadenylation rate is increased to 10-fold of wild type (10×) and a mutant whose deadenylation rate is decreased to 1/10 of wild type (1/10×). The graph is taken from the decay from steady-state program at zero time point.

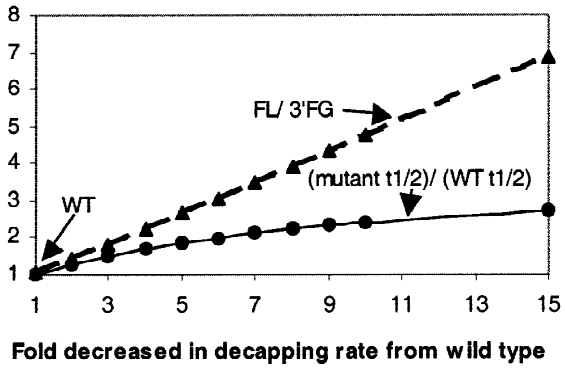

FIGURE 7. Change on half-life and full-length to 3′ fragment ratio (FL/3′FG) at steady-state condition for MFA2pG partial decapping mutants *in silico.* All of the decapping rates (k3, k9, and k10) are changed by the same magnitude simultaneously for *in silico* mutants. The relationship can be fit into this equation with 99% confidence: FL/3′FG = $0.4166X + 0.585 \pm 0.01$. *X* represents the fold decreased on decapping rate.

uted to the slow rate of decapping of the PGK1pG mRNA, which is closer to the rate of 3′-to-5′ decay for this mRNA. As a consequence of this difference between the mRNAs, the effect of decreases in decapping rates is buffered for the PGK1 mRNA. This is a general principle of this network of decay steps, that different mRNAs can be differentially responsive to changes in different steps in the pathway.

A third feature revealed by changes in decapping rates is the relationship between relative 3′ mRNA fragment levels at steady state and the decapping rate. In this case, there is a linear relationship between the change in the decapping rate constant and the ratio of the full-length mRNA to the 3′ fragment at steady state (Fig. 7). This ratio has previously been used to isolate mutants in mRNA turnover (Hatfield et al., 1996) and is a useful indicator of changes in mRNA metabolism. This analysis demonstrates that as long as a specific condition or lesion only affects a single step in decay

TABLE 4. MFA2pG and PGK1pG *in silico* decapping mutants.[a]

	Wild type		10× WT		1/5 WT		1/10 WT		1/100 WT		0	
Category	MFA2	PGK1	MFA2	PGK1	MFA2	PGK1	MFA2	PGK1	MFA2	PGK1	MFA2	PGK1
Half-life	3.8	27.4	2.8	15.7	7.0	42.0	9.1	46.1	13.4	50.8	14.2	51.4
Life span	6	47.3	4.3	28.4	10.7	68.6	14.4	74.6	20.7	81.4	22.1	82.3
Full length	446	3206	334	1856	802	4831	1031	5285	1512	5815	1603	5883
5′ Fragment	0.1	28	3.9	0.13	5	286	15.3	539	138	1377	250	1613
3′ Fragment	428	791	464	1372	302	292	217	164	35	18.4	0	0
A10 FL	101	640	13	175	266	839	334	872	435	905	450	909
A0 FL	25	924	0.4	39	215	2351	377	2772	757	3269	833	3333
Cap-A10 FL	0.8	0.3	1	0.8	0.4	0.08	0.3	0.04	0.03	0.004	0	0
Cap-A0 FL	0.2	0.4	0.03	0.2	0.3	0.2	0.3	0.13	0.06	0.015	0	0
A10 FG	105	213	131	581.5	55	56	35	29	5	3	0	0
A0 FG	323	578	333	790.5	247	236	182	135	30	15	0	0

[a]k3, k9, and k10 are changed by equal magnitude in all mutants.

(such as decapping), then the actual change in the rate constant in vivo can be inferred from the steady-state ratio of the full-length to 3′ mRNA fragment. Moreover, the change in full-length to 3′ fragment ratio is more sensitive than half-life change in response to decapping rate change (see Fig. 7 for comparison); thus it can be a better indicator for mild defects in decapping.

Changes in 5′-to-3′ exonucleolytic decay

The results of changes in the rate of 5′-to-3′ exonucleolytic degradation are shown in Table 5. In general, the effects are similar to decapping mutants. However, because the rate we assigned to 5′-to-3′ exonuclease digestion is much faster than the decapping rate, a larger change in the rate is required to have an effect on mRNA decay parameters (Fig. 5). One difference between inhibiting decapping and 5′-to-3′ exonuclease digestion is the accumulation of different mRNA species. For example, in the decapping mutants, the increase in the full-length amount comes from the accumulation of capped A10 and A0 mRNA. In contrast, inhibiting 5′-to-3′ exonucleolytic decay leads to the accumulation of uncapped A10 and A0 mRNA (compare Table 4 and Table 5).

In a minor point, it should be noted that a change in 5′-to-3′ digestion can lead to a change in the observed 3′ mRNA fragment half-life, when it is measured following cycloheximide addition (Anderson & Parker, 1998). Cycloheximide has been shown to stabilize yeast transcripts by blocking decapping (Beelman & Parker, 1994). It has been used to block decapping, and thus the generation of 3′ fragment from 5′-to-3′ decay to measure the half-life of the 3′ fragment (e.g., Anderson & Parker, 1998). A change in the 3′ fragment half-life from this kind of experiment is often explained by the change on terminal deadenylation or 3′-to-5′ decay rate. However, even when the 3′-to-5′ decay rate and terminal deadenylation rate remain unchanged, the decrease on the rate of 5′-to-3′ exonucleolytic decay will still cause change on the observed fragment half-life (Table 5). This can be understood because the inhibition of 5′-to-3′ decay leads to a continued production of 3′ mRNA fragment even after the inhibition of decapping, and will thus lead to an overestimation of the 3′ mRNA fragment decay rate.

Changes in both deadenylation and decapping rates

Numerous sequence elements that enhance the decay rate of eukaryotic mRNAs are known to stimulate the rates of both deadenylation and subsequent decapping (e.g., Shyu et al., 1991; Caponigro & Parker, 1996; Olivas & Parker, 2000). Given this, we have also modeled the effect on the mRNA decay network of simultaneous changes in these two steps. The most notable difference between these simulations and those above is that a smaller changes in the rate leads to a larger effect on mRNA metabolism (for comparison see Fig. 8). For example, decreasing the rates of both deadenylation and decapping 5-fold led to a 4.8-fold increase in the half-life for the MFA2 mRNA and a 4.1-fold increase in the half-life for the PGK1 mRNA. In contrast, a 5-fold decrease in deadenylation rate for MFA2 gave a 3.8-fold increase in half-life, whereas a 5-fold decrease in decapping rate for MFA2 only gave rise to a 1.8-fold increase in half-life. This larger effect of change in multiple rates can be understood as due to the dependent nature of the steps in the decay pathway and provides a mathematical explanation for why so many decay elements have been identified that promote both steps in the decay pathway.

TABLE 5. MFA2pG and PGK1pG *in silico* 5′-to-3′ exonuclease mutants.

	Wild type		10× WT		1/10 WT		1/100 WT		1/1,000 WT		0 (1/1E10 WT)	
Category	MFA2	PGK1	MFA2	PGK1	MFA2	PGK1	MFA2	PGK1	MFA2	PGK1[a]	MFA2	PGK1
Half-life (min)	3.8	27.4	3.8	27.4	3.8	27.4	4.5	27.9	8.8	32.1	14.2	51.4
Life span (min)	6	47.3	6	47.3	6.2	47.4	7.5	48.5	14.0	57.2	22.0	82.3
Full length	446	3206	446	3205	455	3212	539	3276	1018	3789	1603	5883
5′ Fragment	0.1	28	0.12	28	0.2	29	2	41	58	177	250	1613
3′ Fragment	428	791	428	791	425	788	397	760	223	574	~0	~0
3′FG half-life (min)	14.9	15.0	14.9	15.0	15.0	15.2	16.2	16.4	23.0	25.7	N/A	N/A
A10 FL	101	640	101	640	101	640	101	640	101	640	101	640
A0 FL	25	924	25	924	25	924	25	924	25	924	25	924
Cap-A10 FL	0.8	0.3	0.08	0.03	8	3	64	27	241	140	350	269
Cap-A0 FL	0.2	0.4	0.02	0.04	2	4	30	44	331	444	808	2409
A10 3′ FG	105	213	105	213	103	211	86	192	33	102	~0	~0
A0 3′ FG	323	578	323	578	322	577	311	568	190	472	~0	~0

[a]0.00101 instead of 0.001 is used.

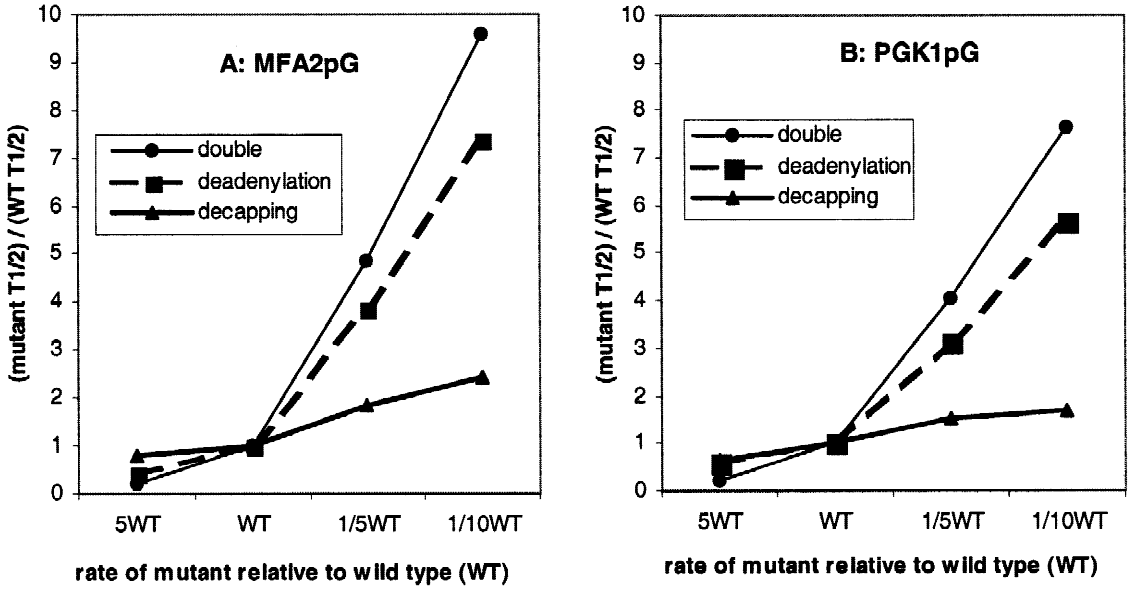

FIGURE 8. Comparison of *in silico* deadenylation, decapping, and deadenylation and decapping double (double) mutants. **A:** MFA2pG. **B:** PGK1pG. For deadenylation and decapping double mutants, r1–r8, k3, k9, and k10 are changed by equal magnitude.

Changes in 3′-to-5′ exonucleolytic decay

The results of changes in the rate of 3′-to-5′ exonucleolytic degradation are shown in Table 6. Several points can be made from this simulation. First, there is essentially no change in the levels or decay rates of either the MFA2 or PGK1 full-length mRNAs when the rate of 3′-to-5′ degradation is either increased or decreased substantially (see Fig. 5 for comparison). The failure of a decrease in 3′-to-5′ degradation rate to affect full-length mRNA decay is simply a consequence of this pathway normally being slower than 5′-to-3′ decay of the mRNAs. Interestingly, we also observed that substantial increases in the rate of 3′-to-5′ degradation also did not affect the rate of full-length mRNA turnover substantially. This can be understood as a consequence of the requirement for terminal deadenylation before 3′-to-5′ degradation can occur. Thus, even when 3′-to-5′ degradation is extremely rapid, the slow rate of terminal deadenylation leads to the mRNAs being degraded by decapping and 5′-to-3′ degradation.

In this light, it should be noted that there is evidence that terminal deadenylation and 3′-to-5′ degradation of the mRNA body are different. Specifically, terminal deadenylation is stimulated by the MFA2 3′ UTR that promotes deadenylation (Muhlrad & Parker, 1992; Decker & Parker, 1993). In addition, terminal deadenylation is faster than 3′-to-5′ decay and appears to have a discrete end point, whereas 3′-to-5′ decay of the body appears to be processive once it starts (Anderson & Parker, 1998). Finally, terminal deadenylation occurs normally in strains defective in 3′-to-5′ decay of the mRNA body (Anderson & Parker, 1998). This analysis predicts that one way to suppress defects in 3′-to-5′ decay would be to increase the rate of terminal deadenylation.

TABLE 6. MFA2pG and PGK1pG *in silico* 3′-to-5′ decay mutants.[a]

	Wild type (WT)		10× WT		1,000× WT		1/10 WT		1/100 WT	
Category	MFA2	PGK1	MFA2	PGK1	MFA2	PGK1[b]	MFA2	PGK1	MFA2	PGK1
Half-life (min)	3.8	27.4	3.7	21.0	3.6	19.3	3.8	32.2	3.8	33.1
Full length	446	3206	433	2485	421	2283	450	3713	450	3796
5′ Fragment	0.1	28	0.5	40	0.05	1	0.01	5	0.001	0.5
3′ Fragment	428	791	133	244	131	213	3426	7869	33426	79849
3′ FG half-life (min)	14.87	15.02	5.49	10.14	5.22	10.42	128.6	116	>15 h	>15 h

[a]k5, k8, and k11 are changed by equal magnitude in all mutants.
[b]1.01 instead of 1 is used for k5 to avoid a special case from happening.

We have also simulated the effects of simultaneously changing the rates of both terminal deadenylation and 3′-to-5′ degradation of the mRNA body. In this case, we also observed minimal change on mRNA decay rates (data not shown). Indeed, only when both rates are increased 100-fold do we see a 2-fold change in the decay rate for the PGK1 mRNA. These results suggest that alterations in the rates of terminal deadenylation and 3′-to-5′ degradation will have little effect on the turnover of yeast mRNAs, which is primarily decayed in the 5′-to-3′ direction. However, it should be noted that there might be specific mRNAs that have a very slow rate of decapping and therefore might be more affected by alterations in these rate constants.

A second interesting point is that the 3′ mRNA fragment produced by 5′-to-3′ decay is a robust indicator of the rate of 3′-to-5′ decay. Decreases and increases in the rate of 3′-to-5′ decay led to predictable changes in the level of the 3′ mRNA fragment at steady state (Fig. 9). It should be noted that this analysis requires the assumption that an alteration in 3′-to-5′ decay directly affects no other steps in the decay network. Because changes in the rate of 3′-to-5′ degradation do not have an effect on the levels of the full-length mRNA at steady state, the ratio of the 3′ mRNA fragment to the full length can be used to calculate the change in the rate constant for 3′-to-5′ degradation. For example, in ski2Δ mutants, which are known to have a defect in 3′-to-5′ degradation, the ratio of 3′ fragment to full-length MFA2pG is 4.3 as compared to 0.9 in wild-type strains (Anderson & Parker, 1998). This predicts that the actual rate of 3′-to-5′ degradation in these mutant strains is changed approximately 5-fold. Similarly for PGK1 mRNA, the ratio changes from 0.3 in wild type to 2.6 in ski2Δ strains. This predicts a 12-fold decrease in the rate of 3′-to-5′ degradation for the mRNA fragment from PGK1pG. The reason for this predicted difference between these two mRNAs is not clear at this time.

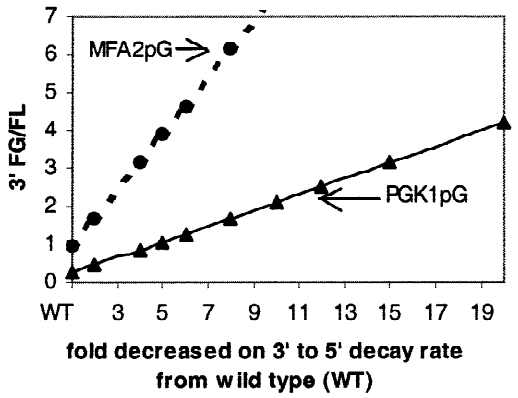

FIGURE 9. The relationship between 3′-to-5′ decay rate change and 3′ fragment to full-length ratio (3′FG/FL) at the steady-state condition. All of the 3′-to-5′ decay rates (k5, k8, and k11) are changed by same magnitude simultaneously for *in silico* mutants.

DISCUSSION

In this work, we have developed a computational model of eukaryotic mRNA turnover. This model is based on substantial knowledge of the discrete steps in the mRNA degradation process derived from previously published experiments. The validity of the model is underscored by the fact that, using rate constants derived from published experiments, this model closely reproduces the observed data. An important point is that this computational model should be applicable to any eukaryotic cell with the same pathways of mRNA degradation. The model can be adapted to other organisms by changing the various rate constants, the length of the initial poly(A) tail, and the efficiency or absence of the poly(G) tract.

This model can be used in a variety of manners. The programs can be utilized to predict how changes in various rates will affect the turnover of individual mRNAs. It can be used to predict the steady-state distribution, half-life, and pulse-chase gel pattern of transcripts under previously uncharacterized mutant conditions, providing there is sufficient data to estimate the various rate constants. In many cases, individual rate constants can be initially estimated from the overall decay rate and steady-state poly(A) tail distribution. Examination of the *in silico* predictions for such initial rate constants can reveal discrepancies that can be resolved by experiments or numerical refinement. After obtaining a realistic model for a given transcript, the modeling work can offer a more quantitative analysis on the decay network. The modeling work can also be utilized to suggest the best experiment for a particular purpose. For example, our analysis suggests that a partial inhibition of decapping rate will be more clearly revealed in a measurement of full-length to 3′ mRNA fragment ratio at steady state, as compared to a pulse-chase experiment or measurement of mRNA half-life. As an example of one of the applications, we have utilized this program to examine the properties of this mRNA decay network system under both normal conditions and when various rates are altered. This work has led to a number of insights into the properties of the system of mRNA turnover and the interpretation of experimental data. These are discussed in detail below.

"Half-life" is not the average life span of eukaryotic mRNAs

Our results suggest that the "half-life" of an mRNA as traditionally measured underestimates the time an mRNA actually persists in the cell. This is a consequence of the fact that the distinct steps in the mRNA decay pathway reveal that mRNA decay is not a simple first-order process. However, a common experimental approach in the analysis of mRNA turnover is the mea-

surement of the mRNA half-life based on the decay of mRNA levels from steady state following the inhibition of new mRNA synthesis. This "half-life" value is then interpreted to represent the average time an mRNA is present in the cell before degradation. This approach underestimates the time an mRNA persists in the cell because at steady state, the mRNAs are already distributed into later steps in the decay pathway. This can be seen by the difference in half-life as computed from the traditional decay from steady-state simulations as compared to the average life span calculated from the *in silico* pulse-chase experiments. For example, the half-lives of the MFA2pG and PGK1pG mRNAs are 3.8 and 27.4 min, respectively, whereas the average life spans are 6 and 47.3 min, respectively. Thus, the average life span is approximately 1.6-fold longer for MFA2 and 1.7-fold longer for PGK1. The fundamental reason for these differences is that at steady-state conditions, the mRNAs are distributed at all phases of the decay pathway, and therefore a certain percentage have already passed steps that might contribute to the overall life span. In contrast, in the pulse-chase experiment, the average time it takes an mRNA to complete all the required steps of mRNA turnover are measured, thereby giving a more accurate measure of the time an mRNA persists within the cell. An interesting point is that for different transcripts, the half-life or average life span may be more relevant. For example, for a transcript that is continually expressed and then only transiently shut off, the half-life will be the relevant biological value for the regulatory loop in place. In contrast, mRNAs that are only transiently expressed such as the c-fos mRNA in response to serum stimulation, the average life span may be a more accurate measurement of the relevant biological expression time.

Individual mRNAs will be differentially affected by changes in specific rates

Our analysis indicates that a measurement of decay from steady state can predominantly measure different rate constants for different mRNAs. This is another consequence of the distribution of individual mRNAs into different stages of the decay pathway at steady state. For example, consider an mRNA with a rapid deadenylation rate but a slow decapping rate. This mRNA accumulates at steady state as a deadenylated species and subsequent measurement of decay is predominated by the decapping rate. In contrast, for a mRNA with a slow deadenylation rate and very rapid decapping, the rate of decay from a steady-state population is predominated by the rate of deadenylation. In essence, these two hypothetical mRNAs have different rate-limiting steps in the pathway of decay. A corollary of these differences is that individual mRNAs will respond differentially to changes in generic steps in the decay pathway. As an example of this effect, PGK1 is less responsive to changes in transport rate than MFA2 because the decay steps following transport are slower for PGK1 than MFA2 (Fig. 4). Given this, mRNA-specific effects due to mutations should not be considered proof of a specific involvement in the turnover of a limited subset of mRNAs.

Deadenylation is the key step in controlling turnover

Our simulations argue that the modulation of deadenylation is the most effective manner of controlling mRNA decay rates. This is based on the comparison of the effects of changes in mRNA decay rates when deadenylation, decapping, or 3′-to-5′ decay are altered (Fig. 5). We observed that the largest changes in overall mRNA half-life or average life span were obtained with changes in deadenylation rate. This effect can be understood because deadenylation is a required step for both decapping and 3′-to-5′ degradation, and because the entire process of deadenylation is overall one of the slowest steps in the overall process. Given this mathematical dependence, it is not surprising that a large amount of biological regulation occurs at the step of controlling deadenylation rate (for a review, see Gray & Wickens, 1998). It should also be noted that the poly(A) tail can affect translation initiation rate as well (for a review, see Jacobson, 1996; Sachs et al., 1997). Thus, differential control of deadenylation will not only have the largest effect on mRNA decay rates but may also have a synergistic effect on the rate of protein production. Given these effects, the modulation of deadenylation rates will be a critical step in controlling mRNA metabolism.

Implications for the process of 3′-to-5′ degradation of mRNA

Our simulations argue that individual mRNAs can show different rates of 3′-to-5′ degradation. This is based on the calculations that the rates of 3′-to-5′ degradation of MFA2pG and PGK1pG mRNAs are different. This is also consistent with experimental results that show that the decay rates of the MFA2 and PGK1 mRNAs are different in dcp1Δ strains (Anderson & Parker, 1998). However, these observed differences could have been due to differences in the deadenylation rates of these two different mRNAs. In our simulations we have accurately controlled for this difference and were forced to assign different values of 3′-to-5′ decay for these two mRNAs to match the observed experimental data. Given this, we estimate that the PGK1 mRNA is degraded fourfold slower than the MFA2 mRNA by the 3′-to-5′ decay system.

Interestingly, two observations suggest that the mRNA fragments produced by 5′-to-3′ degradation of the MFA2 and PGK1 mRNAs are degraded at the same rate by

the 3′-to-5′ degradation machinery. First, these mRNA fragments show identical decay rates in experiments (Anderson & Parker, 1998). Second, in our simulations, the value assigned to the 3′-to-5′ decay of the mRNA fragment was almost identical for these two transcripts. This suggests that the differences between the 3′-to-5′ decay rates for the full-length mRNAs are a consequence of features of the body of the mRNA and are not simply specified by the 3′ UTR elements. Moreover, because the rate of 3′-to-5′ degradation of the PGK1 fragment is faster than the 3′-to-5′ degradation of the full-length mRNA, it suggests that a functional mRNA can protect the 3′ end from exonucleolytic attack, possibly by interactions between the 5′ and 3′ termini.

An increase in the transcript amount may not necessarily produce a correspondent increase in the protein yield

Our mutant analysis with this program suggests that sometimes a significant increase in the transcript amount detectable by northern hybridization or DNA microarray may not produce a correspondent increase in the protein yield. For example, in the *in silico* transport mutants, the increase in the full-length transcript level solely comes from an increase in the nuclear transcripts (Table 2). Similarly, for 5′-to-3′ exonuclease mutants, the increase in the full-length transcript amount solely comes from an increase in an uncapped mRNA (Table 5). Because translation is thought to begin in the cytoplasm, and the cap structure is thought to be required for efficient translation initiation, the nuclear mRNA and uncapped mRNA are likely to be not as competent for translation as other mRNA species. Thus it may not lead to a correspondent increase in the protein yield. Nevertheless, it should be noted that in most cases, one would expect a correlation of mRNA levels with protein production.

Future modeling of mRNA biogenesis and function

In summary, we have constructed an mRNA biogenesis and degradation simulator, with a focus on the mRNA degradation process. To our knowledge, this is the first computational model applied to the larger issues of mRNA biogenesis, function, and degradation. Given this first step, there are several improvements that can be made in the future. For example, it would be ideal to create a robust mRNA biogenesis and function predictor that includes additional steps in mRNA biogenesis, such as RNA processing, and function, including translation rate and protein production. One technical difficulty in this goal is that an increase in complexity of the mathematical model will essentially prevent the direct solving of the differential equations. Given this limitation, future modeling will need to take the input of equations (such as in Appendix 1), parse them directly into computer recognizable code, and solve the equations numerically. This approach will allow for more complex mathematical constructs and will also speed the analysis of the modeling result.

There are several additional difficulties to be overcome in developing such a more integrated model of mRNA biogenesis and function. First, additional information must be obtained on the specific steps in RNA metabolism including their order and dependencies, as well as branch pathways that lead to altered downstream events or premature mRNA degradation. Second, sufficient experimental data needs to be obtained to allow the measurement or estimation of rate constants. Ideally, this latter type of data will be obtained from genomic analyses that should also reveal mRNA-specific differences, which may provide insights into posttranscriptional control mechanisms.

METHODS

Mathematical description of mRNA levels

To describe the amount of the different mRNA species as a function of time, we needed to describe the amount of each species in an equation based on the various rate constants. Our approach was to describe the amount of each species as a function of the rate constants that both give rise to that species and lead to decay of the species using a series of ordinary differential equations. For a general scheme like this: $\xrightarrow{k_{in(1)}} X_1 \xrightarrow{k_{out(1)}} \cdots \xrightarrow{k_{in(i-1)}} X_{i-1} \xrightarrow{k_{in(i)} \text{ or } k_{out(i-1)}} X_i \xrightarrow{k_{out(i)}}$, we assume both the degradation and the generation of component X are first-order process here. If $X_i(t)$ represents the quantity of component i at time t, $X_{i-1}(t)$ represent the quantity of component $i-1$ at time t, $k_{in(i)}$ is the summation of rate constants that generate X_i from component X_{i-1}, and $k_{out(i)}$ is the summation of rate constants that degrade X_i, the following equation can be directly derived:

$$dX_i(t) = k_{in(i)} X_{i-1}(t)dt - k_{out(i)} X_i(t)dt. \quad (1)$$

The analytical solution of Equation 1 can be expressed as the following general formula:

$$X_i = SS_i + \sum_{j=1}^{i} A_j e^{-k_{out(j)} t} \quad (2)$$

where

$$SS_i = \frac{k_{in(1)} k_{in(2)} \cdots k_{in(i-1)} k_{in(i)}}{k_{out(1)} k_{out(2)} \cdots k_{out(i-1)} k_{out(i)}}$$

$$A_j = f(Aj(0), k_{in(j)}, k_{out(j)}).$$

The first term for Equation 2 (SS_i) represents the steady-state level of component i, which is equal to the product of rate constants for generation of every component precedes component i divided by the product of rate constants at which

every component precedes *i* degrades. The coefficient A_j for the exponential term is a function of the initial amount of every component precedes *i*, and the rate constants that generate every component and the rate constants that degrade them. The root for the exponential term is a function of the rate at which every component precedes *i* degrades and the time *t*.

If we assume transcription is a zeroth-order process and all the others are first-order processes, we can mathematically describe the amount of each species in the model in Figure 1 by a series of ordinary differential equations using the same approach as above. The complete detailed equations and their solutions are shown in Appendix 1 and 2, respectively. The correctness and accuracy of the math solution has been tested by Matlab trial version 6. Examination of the solutions (shown in Appendix 2) indicates that when some of the rate constants are equal, some coefficients will reach an infinite value because the denominator is zero. Under these circumstances, the solution is another set of more complicated equations. However, because these equations greatly complicate the computer programming, we suggest using a very small difference in the rate constants for those that are intended to be equal to avoid this situation. We have tested by Matlab that a small difference between the rate constants estimated is close enough to the modeling result of equal rate constants (data not shown).

Estimation of rate constants for MFA2pG and PGK1pG

The rate constants we utilized for modeling the decay of the MFA2pG and PGK1pG transcripts are based on the experimental evidence and logic outline below (also shown in Table 1).

Transcription rate

From the solutions (Appendix 2), we can conclude that the rate of transcription (k1) will not affect the half-life and the ratios between individual species in the decay network. This is because k1 is never at the root of the exponential term, thus k1 will not affect the half-life calculation. In addition, k1 is in the first term of every equation, which represents the steady-state level of every intermediate, so when we get the ratio of any two intermediates by dividing them, k1 will be eliminated. We arbitrarily set the transcription rate to 1 U/s in our following simulation, which means transcription will generate 1 transcript per second. The value of k1 can be easily changed to alter the amount of transcripts in the simulation. This can be a useful technique to "darken" or "lighten" the virtual northern gel output.

Transport and 5′-to-3′ exonuclease rate

We also assigned a relatively large rate for 5′-to-3′ exonuclease (k4) and for transport rate (k2). We did this because the intermediates from these two processes are present at low levels, suggesting these two processes are fast. We utilized a transport rate that gives an ~1% transcript distributed in the nucleus for MFA2pG. We also use the same transport rate for PGK1pG, thereby assuming in this modeling that all mRNAs are transported at the same rate. It should be noted that the actual rates of these two processes are essentially unknown.

Poly(A) shortening rates

The rates for poly(A) shortening (r1–r6, r8) are based on the published results from the measurement on high-resolution northern gels for PGK1 and MFA2 transcripts in a transcriptional pulse-chase experiment (Decker & Parker, 1993; Muhlrad et al., 1994, 1995). In each case, the rate is calculated as the reciprocal of the time (seconds) for the synchronous pulse of transcript to complete poly(A) tail shortening within certain range of A tail length. Specifically, it takes about 90 s for the initial deadenylation process (70A–60A) in MFA2pG, so r1 is equal to 1/90 s^{-1} which is about 0.011 s^{-1}. Subsequently, it takes about 3.75 min for the MFA2pG poly(A) tail to shorten from 60A to 10A. Because we assume the poly(A) shortening process is roughly constant from 60A–10A, each 10 adenosine residues are calculated to be removed in about 45 s (3.75/5 min). This yields r2 to r6 with values of about 0.0222 (1/45) s^{-1}. We add a small difference between r2 and r6 here to avoid the exceptional case for the simulator. We performed a similar rate constant assignment for PGK1pG, which in total takes about 30 min for poly(A) tail shortening from 70A to 10A.

Terminal deadenylation rates on mRNA fragments (r8) can also be measured from transcriptional pulse-chases experiments (Schwartz & Parker, 1999, 2000). In this case, it takes about 7.5 min for terminal deadenylation of the MFA2pG 3′ fragment, which gives r8 a value of about 0.00222 (1/7.5 × 60) s^{-1}. Terminal deadenylation for the PGK1pG 3′ fragment requires about 15 min (D. Schwartz & R. Parker, unpubl. observations), yielding r8 for PGK1pG of about 0.0011 (1/900) s^{-1}. It has been difficult to directly measure terminal deadenylation on full-length mRNAs. Given this, we assumed that terminal deadenylation is the same rate on full-length (r7) and 3′ fragments (r8). At the current time this is consistent with the available experimental data, but it is an explicit assumption of our modeling.

Decapping rates

The decapping rate (k3) is estimated from the decay rate of the oligoadenylated mRNAs in transcriptional pulse-chase experiments (Decker & Parker, 1993; Muhlrad et al., 1994, 1995). The half-life of the oligoadenylated mRNA for MFA2pG is about 90 s, this assigns k3 a value of ~0.0077 (ln2/90 = 0.693/90) s^{-1}. Similarly, the k3 for PGK1pG is about 0.00462 (0.693/1500) s^{-1}, as the half-life for its oligoadenylated mRNA is about 25 min. Experimental evidence is consistent with the A10–A0 tail not affecting decapping rate. Therefore, we assume that the decapping rate for A0 transcript is the same as that for A oligo full length (Decker & Parker, 1993); thus k9 = k3. Essentially no information is available about the decapping rate for mRNAs that have been digested 3′ to 5′ to the internal poly(G) tract. We find in our simulation that if we adjust this rate (k10) to be 10-fold faster than k3 (see the Results for discussion), the steady-state level of 5′ fragment relative to full length is more consistent with the experimental

data (Beelman et al., 1996). It should be noted that this particular rate constant (k10) is solely based on *in silico* calculations.

3′-to-5′ exonucleolytic decay

The rate of 3′-to-5′ decay for fragment (k5) is adjusted to give the correct fragment half-life of 15 min for both PGK1pG and MFA2pG as published (Anderson & Parker, 1998). In this case, we developed a program that simulates the measurement of fragment half-life by cycloheximide (Anderson & Parker, 1998). In this program, every component starts from the steady-state level. The transcription rate and decapping rate are then changed to zero, comparable to transcription repression in the presence of cycloheximide, which blocks decapping in laboratory conditions (Beelman & Parker, 1994). We then adjusted k5 to get the observed 15 min of fragment half-life. This gives us a k5 of 0.0009 for MFA2pG and 0.001 for PGK1pG. The k5 for PGK1pG is slightly higher because another degradation rate for fragment (r8) is slower for PGK1pG. The rate of 3′-to-5′ decay for full length (k8) is estimated based on the rate of decay of the deadenylated full-length mRNAs in a dcp1Δ strain, wherein decapping is blocked and mRNAs can only be degraded by the 3′-to-5′ decay pathway. In the decay from steady-state program we set the decapping rate to zero, then adjust k8 to get a full-length half-life of about 14 min for MFA2pG and of about 51 min for PGK1pG (Dunckley & Parker, 1999). This is an example of how the programs can be used to derive specific rate constants where a variety of information is available.

ACKNOWLEDGMENTS

We thank Jian Yang for directing us to Java applet and his assistance on debugging the code. We also thank Dr. Daniel Herschlag and members of R.P.'s laboratory for critical reading and constructive comments on the manuscript. This work was supported by a grant to R.P. from the National Institutes of Health (GM45443) and by funds from the Howard Hughes Medical Institute.

Received March 9, 2001; returned for revision
April 26, 2001; revised manuscript received
May 24, 2001

REFERENCES

Anderson JSJ, Parker R. 1998. The 3′ to 5′ degradation of yeast mRNAs is a general mechanism for mRNA turnover that requires the SKI2 DEVH box protein and 3′ to 5′ exonucleases of the exosome complex. *EMBO J 17*:1497–1506.

Beelman CA, Parker R. 1994. Differential effects of translational inhibition *in cis* and *in trans* on the decay of the unstable yeast MFA2 mRNA. *J Biol Chem 269*:9687–9692.

Beelman CA, Parker R. 1995. Degradation of mRNA in eukaryotes. *Cell 81*:179–183.

Beelman CA, Stevens A, Caponigro G, LaGrandeur TE, Hatfield L, Fortner DM, Parker R. 1996. An essential component of the decapping enzyme required for normal rates of mRNA decay in yeast. *Nature 382*:642–646.

Boeck R, Lapeyre B, Brown CE, Sachs AB. 1998. Capped mRNA degradation intermediates accumulate in the yeast spb8-2 mutant. *Mol Cell Biol 18*:5062–5072.

Bousquet-Antonelli C, Presutti C, Tollervey D. 2000. Identification of a regulated pathway for nuclear pre-mRNA turnover. *Cell 102*: 765–775.

Brown CE, Sachs AB. 1998. Poly (A) tail length control in *Saccharomyces cerevisiae* occurs by message-specific deadenylation. *Mol Cell Biol 18*:6548–6559.

Caponigro G, Parker R. 1996. mRNA turnover in yeast promoted by the MATα1 instability element. *Nucleic Acids Res 24*:4304–4312.

Decker CJ, Parker R. 1993. A turnover pathway for both stable and unstable mRNAs in yeast: Evidence for a requirement for deadenylation. *Genes & Dev 7*:1632–1643.

Dunckley T, Parker R. 1999. The DCP2 protein is required for mRNA decapping in *Saccharomyces cerevisiae* and contains a functional Mut motif. *EMBO J 18*:5411–5422.

Gray NK, Wickens M. 1998. Control of translation initiation in animals. *Annu Rev Cell Dev Biol 14*:399–458.

Hatfield L, Beelman CA, Stevens A, Parker R. 1996. Mutations in *trans*-acting factors affecting mRNA decapping in *Saccharomyces cerevisiae*. *Mol Cell Biol 16*:5830–5838.

Hilleren P, Parker R. 1999. Mechanisms of mRNA surveillance in eukaryotes. *Annu Rev Genet 33*:229–260.

Hilleren P, Parker R. 2001. Defects in the mRNA export factors Rat7p, Gle1p, Mex67p, and Rat8p cause hyperadenylation during 3′ end formation of nascent transcripts. *RNA 7*:753–764.

Jacobson A. 1996. Poly (A) metabolism and translation: The closed-loop model. In: J.W.B. Hershey, ed. *Translational control.* Cold Spring Harbor, New York: Cold Spring Harbor Laboratory Press. pp 451–480.

Muhlrad D, Decker CJ, Parker R. 1994. Deadenylation of the unstable mRNA encoded by the yeast *MFA2* gene leads to decapping followed by 5′ → 3′ digestion of the transcript. *Genes & Dev 8*:855–866.

Muhlrad D, Decker CJ, Parker R. 1995. Turnover mechanisms of the stable yeast PGK1 mRNA. *Mol Cell Biol 15*:2145–2156.

Muhlrad D, Parker R. 1992. Mutations affecting stability and deadenylation of the yeast MFA2 transcript. *Genes & Dev 6*:2100–2111.

Muhlrad D, Parker R. 1999. Aberrant mRNAs with extended 3′UTR are substrates for rapid degradation by mRNA surveillance. *RNA 5*:1299–1307.

Neville M, Rosbash M. 1999. The NES-Crm1p export pathway is not a major mRNA export route in *Saccharomyces cerevisiae*. *EMBO J 18*:3746–3756.

Olivas W, Parker R. 2000. The Puf3 protein is a transcript-specific regulator of mRNA degradation in yeast. *EMBO J 19*:6602–6611.

Parker R, Herrick D, Peltz SW, Jacobson A. 1991. Measurement of mRNA decay rates in *Saccharomyces cerevisiae*. *Methods Enzymol 194*:415–423.

Sachs AB, Sarnow P, Hentze MW. 1997. Starting at the beginning, middle and end: Translation initiation in eukaryotes. *Cell 89*: 831–838.

Schwartz DC, Parker R. 1999. Mutations in translation initiation factors lead to increased rate of deadenylation and decapping of yeast mRNAs. *Mol Cell Biol 19*:5247–5256.

Schwartz DC, Parker R. 2000. mRNA decapping in yeast requires dissociation of the cap binding protein, eukaryotic translation initiation factor 4E. *Mol Cell Biol 20*:7933–7942.

Shyu AB, Belasco JG, Greenberg ME. 1991. Two distinct destabilizing elements in the c-fos message trigger deadenylation as a first step in rapid mRNA decay. *Genes & Dev 5*:221–231.

Tharun S, He W, Mayes AE, Lennertz P, Beggs JD, Parker R. 2000. Yeast Sm-like proteins function in mRNA decapping and decay. *Nature 404*:515–518.

Tucker M, Valencia-Sanchez MA, Staples R, Chen J, Denis CL, Parker R. 2001. The transcription factor associated Ccr4 and Caf1 proteins are components of the major cytoplasmic mRNA deadenylase in *Saccharomyces cerevisiae*. *Cell 104*:377–386.

Vreken P, Raue HA. 1992. The rate-limiting step in yeast PGK1 mRNA degradation is an endonucleolytic cleavage in the 3′ terminal part of the coding region. *Mol Cell Biol 12*:2986–2996.

APPENDIX 1

The following equations are derived from the model described in Figure 1:

$$dA(t) = k1dt - (k2 + k6)A(t)dt$$

$$dB(t) = k2A(t)dt - k7B(t)dt - r1B(t)dt$$

$$dBC1(t) = r1B(t)dt - r2BC1(t)dt$$

$$dBC2(t) = r2BC1(t)dt - r3BC2(t)dt$$

$$dBC3(t) = r3BC2(t)dt - r4BC3(t)dt$$

$$dBC4(t) = r4BC3(t)dt - r5BC4(t)dt$$

$$dBC5(t) = r5BC4(t) - r6BC5(t)dt$$

$$dC(t) = r6BC5(t) - (k3 + r7)C(t)dt$$

$$dD(t) = k3C(t)dt - (k4 + r7)D(t)dt$$

$$dE(t) = r7C(t)dt - (k8 + k9)E(t)dt$$

$$dF(t) = k9E(t)dt + r7D(t)dt - (k4 + k8)F(t)dt$$

$$dG(t) = pG3^{*}k8E(t)dt - (k10 + k11)G(t)dt$$

$$dI1(t) = pG5^{*}k4F(t)dt - k5I1(t)dt$$

$$dL(t) = pG5^{*}k4D(t)dt - r8L(t)dt$$

$$dI2(t) = r8L(t)dt - k5I2(t)dt$$

$$dM(t) = k10G(t)dt + pG3^{*}k8F(t)dt - (k4 + k11)M(t)dt$$

APPENDIX 2

The analytical solutions of the equations in Appendix 1 are shown below and are used in the computer program.

$A = m_a + r_a e^{-(k2+k6)t}$, where

$$m_a = \frac{k1}{k2 + k6} \qquad r_a = A_0 - m_a \ .$$

$B = m_b + n_b e^{-(k2+k6)t} + r_b e^{-(r1+k7)t}$, where

$$m_b = \frac{k2m_a}{r1 + k7} \qquad n_b = \frac{k2r_a}{(r1 + k7) - (k2 + k6)}$$

$$r_b = B_0 - m_b - n_b \ .$$

$BC1 = m_{bc1} + n_{bc1}e^{-(k2+k6)t} + o_{bc1}e^{-(r1+k7)t} + r_{bc1}e^{-r2t}$, where

$$m_{bc1} = \frac{r1m_b}{r2} \qquad n_{bc1} = \frac{r1n_b}{r2 - (k2 + k6)}$$

$$o_{bc1} = \frac{r1rb}{r2 - (r1 + k7)}$$

$$r_{bc1} = BC1_0 - m_{bc1} - n_{bc1} - o_{bc1}.$$

*pG5 represents the efficiency of the poly(G) structure to block 5′-to-3′ exonuclease. pG3 represents the efficiency of the poly(G) structure to block 3′-to-5′ decay. Both of them are between 0 (no blocking effect at all or no poly(G) structure present) and 1 (complete block).

$BC2 = m_{bc2} + n_{bc2}e^{-(k2+k6)t} + o_{bc2}e^{-(r1+k7)t} + p_{bc2}e{-r^{2}t} + r_{bc2}e^{-r3t}$, where

$$m_{bc2} = \frac{r2m_{bc1}}{r3} \qquad n_{bc2} = \frac{r2n_{bc1}}{r3 - (k2 + k6)}$$

$$o_{bc2} = \frac{r2o_{bc1}}{r3 - (r1 + k7)} \qquad p_{bc2} = \frac{r2r_{bc1}}{r3 - r2}$$

$$r_{bc2} = BC2_0 - m_{bc2} - n_{bc2} - o_{bc2} - p_{bc2}.$$

$BC3 = m_{bc3} + n_{bc3}e^{-(k2+k6)t} + o_{bc3}e^{-(r1+k7)t} + p_{bc3}e^{-r2t} + q_{bc3}e^{-r3t} + r_{bc3}e^{-r4t}$, where

$$m_{bc3} = \frac{r3m_{bc2}}{r4} \qquad n_{bc3} = \frac{r3n_{bc2}}{r4 - (k2 + k6)}$$

$$o_{bc3} = \frac{r3o_{bc2}}{r4 - (r1 + k7)} \qquad p_{bc3} = \frac{r3p_{bc2}}{r4 - r2}$$

$$q_{bc3} = \frac{r3r_{bc2}}{r4 - r3}$$

$$r_{bc3} = BC3_0 - m_{bc3} - n_{bc3} - o_{bc3} - p_{bc3} - q_{bc3}.$$

$BC4 = m_{bc4} + n_{bc4}e^{-(k2+k6)t} + o_{bc4}e^{-(r1+k7)t} + p_{bc4}e^{-r2t} + q_{bc4}e^{-r3t} + s_{bc4}e^{-r4t} + r_{bc4}e^{-r5t}$, where

$$m_{bc4} = \frac{r4m_{bc3}}{r5} \qquad n_{bc4} = \frac{r4n_{bc3}}{r5 - (k2 + k6)}$$

$$o_{bc4} = \frac{r4o_{bc3}}{r5 - (r1 + k7)} \qquad p_{bc4} = \frac{r4p_{bc3}}{r5 - r2}$$

$$q_{bc4} = \frac{r4q_{bc3}}{r5 - r3} \qquad S_{bc4} = \frac{r4r_{bc3}}{r5 - r4}$$

$$r_{bc4} = BC4_0 - m_{bc4} - n_{bc4} - o_{bc4} - p_{bc4} - q_{bc4} - s_{bc4}.$$

$BC5 = m_{bc5} + n_{bc5}e^{-(k2+k6)t} + o_{bc5}e^{-(r1+k7)t} + p_{bc5}e^{-r2t} + q_{bc5}e^{-r3t} - s_{bc5}e^{-r4t} + t_{bc5}e^{-r5t} + r_{bc5}e^{-r6t}$, where

$$m_{bc5} = \frac{r5m_{bc4}}{r6} \qquad n_{bc5} = \frac{r5n_{bc4}}{r6 - (k2 + k6)}$$

$$o_{bc5} = \frac{r5o_{bc4}}{r6 - (r1 + k7)} \qquad p_{bc5} = \frac{r5p_{bc4}}{r6 - r2}$$

$$q_{bc5} = \frac{r5q_{bc4}}{r6 - r3} \qquad s_{bc5} = \frac{r5s_{bc4}}{r6 - r4} \qquad t_{bc5} = \frac{r5r_{bc4}}{r6 - r5}$$

$$r_{bc5} = BC5_0 - m_{bc5} - n_{bc5} - o_{bc5} - p_{bc5} - q_{bc5} - s_{bc5} - t_{bc5}.$$

$C = m_c + n_c e^{-(k2+k6)t} + o_c e^{-(r1+k7)t} + p_c e^{-r2t} + q_c e^{-r3t} + s_c e^{-r4t} + t_c e^{-r5t} + u_c e^{-r6t} + r_c e^{-(k3+r7)t}$, where

$$m_c = \frac{r6 m_{bc5}}{k3 + r7} \qquad n_c = \frac{r6 n_{bc5}}{(k3 + r7) - (k2 + k6)}$$

$$o_c = \frac{r6 o_{bc5}}{(k3 + r7) - (r1 + k7)} \qquad p_c = \frac{r6 p_{bc5}}{(k3 + r7) - r2}$$

$$q_c = \frac{r6 q_{bc5}}{(k3 + r7) - r3} \qquad s_c = \frac{r6 s_{bc5}}{(k3 + r7) - r4}$$

$$t_c = \frac{r6 t_{bc5}}{(k3 + r7) - r5} \qquad u_c = \frac{r6 r_{bc5}}{(k3 + r7) - r6}$$

$$r_c = C0 - m_c - n_c - o_c - p_c - q_c - s_c - t_c - u_c.$$

$D = m_d + n_d e^{-(k2+k6)t} + o_d e^{-(r1+k7)t} + p_d e^{-r2t} + q_d e^{-r3t} + s_d e^{-r4t} + t_d e^{-r5t} + u_d e^{-r6t} + v_d e^{-(k3+r7)t} + r_d e^{-(k4+r7)t}$, where

$$m_d = \frac{k3 m_c}{(k4 + r7)} \qquad n_d = \frac{k3 n_c}{(k4 + r7) - (k2 + k6)}$$

$$o_d = \frac{k3 o_c}{(k4 + r7) - (r1 + k7)} \qquad p_d = \frac{k3 p_c}{(k4 + r7) - r2}$$

$$q_d = \frac{k3 q_c}{(k4 + r7) - r3} \qquad s_d = \frac{k3 s_c}{(k4 + r7) - r4}$$

$$t_d = \frac{k3 t_c}{(k4 + r7) - r5} \qquad u_d = \frac{k3 u_c}{(k4 + r7) - r6}$$

$$v_d = \frac{k3 r_c}{(k4 + r7) - (k3 + r7)}$$

$$rd = D0 - m_d - n_d - o_d - p_d - q_d - s_d - t_d - u_d - v_d.$$

$E = m_e + n_e e^{-(k2+k6)t} + o_e e^{-(r1+k7)t} + p_e e^{-r2t} + q_e e^{-r3t} + s_e e^{-r4t} + t_e e^{-r5t} + u_e e^{-r6t} + v_e e^{-(k3+r7)t} + r e^{-(k8+k9)t}$, where

$$m_e = \frac{r7 m_c}{k8 + k9} \qquad n_e = \frac{r7 n_c}{k8 + k9 - (k2 + k6)}$$

$$o_e = \frac{r7 o_c}{k8 + k9 - (r1 + k7)} \qquad p_e = \frac{r7 p_c}{k8 + k9 - r2}$$

$$q_e = \frac{r7 q_c}{k8 + k9 - r3} \qquad s_e = \frac{r7 s_c}{k8 + k9 - r4}$$

$$t_e = \frac{r7 t_c}{k8 + k9 - r5} \qquad u_e = \frac{r7 u_c}{k8 + k9 - r6}$$

$$v_e = \frac{r7 r_c}{k8 + k9 - (k3 + r7)}$$

$$r_e = E0 - m_e - n_e - o_e - p_e - q_e - s_e - t_e - u_e - v_e.$$

$F = m_f + n_f e^{-(k2+k6)t} + o_f e^{-(r1+k7)t} + p_f e^{-r2t} + q_f e^{-r3t} + s_f e^{-r4t} + t_f e^{-r5t} + u_f e^{-r6t} + v_f e^{-(k3+r7)t} + w_f e^{-(k8+k9)t} + x_f e^{-(k4+k7)t} + r_f e^{-(k4+r8)t}$, where

$$m_f = \frac{k9 m_e + r7 m_d}{k4 + k8} \qquad n_f = \frac{k9 n_e + r7 n_d}{(k4 + k8) - (k2 + k6)}$$

$$o_f = \frac{k9 o_e + r7 o_d}{k4 + k8 - (r1 + k7)} \qquad p_f = \frac{k9 p_e + r7 p_d}{k4 + k8 - r2}$$

$$q_f = \frac{k9 q_e + r7 q_d}{k4 + k8 - k3} \qquad s_f = \frac{k9 s_e + r7 s_d}{k4 + k8 - r4}$$

$$t_f = \frac{k9 t_e + r7 t_d}{k4 + k8 - k5} \qquad u_f = \frac{k9 u_e + r7 u_d}{k4 + k8 - r6}$$

$$v_f = \frac{k9 v_e + r7 v_d}{k4 + k8 - (k3 + r7)} \qquad w_f = \frac{k9 r_e}{k4 - k9} \qquad x_f = \frac{r7 r_d}{k8 - r7}$$

$$r_f = F0 - m_f - n_f - o_f - p_f - q_f - s_f - t_f - u_f - v_f - w_f - x_f.$$

$L = m_l + n_l e^{-(k2+k6)t} + o_l e^{-(r1+k7)t} + p_l e^{-r2t} + q_l e^{-r3t} + s_l e^{-r4t} + t_l e^{-r5t} + u_l e^{-r6t} + v_l e^{-(k3+r7)t} + w_l e^{-(k4+r7)t} + r_l e^{-r8t}$, where

$$m_l = pG5 * \frac{k4 m_d}{r8} \qquad n_l = pG5 * \frac{k4 n_d}{r8 - (k2 + k6)}$$

$$o_l = pG5 * \frac{k4 o_d}{r8 - (r1 + k7)} \qquad p_l = pG5 * \frac{k4 p_d}{r8 - r2}$$

$$q_l = pG5 * \frac{k4 q_d}{r8 - r3} \qquad s_l = pG5 * \frac{k4 s_d}{r8 - r4}$$

$$t_l = pG5 * \frac{k4 t_d}{r8 - r5} \qquad u_l = pG5 * \frac{k4 u_d}{r8 - r6}$$

$$v_l = pG5 * \frac{k4 v_d}{r8 - (k3 + r7)} \qquad w_l = pG5 * \frac{k4 r_d}{r8 - (k4 + r7)}$$

$$r_l = L0 - m_l - n_l - o_l - p_l - q_l - s_l - t_l - u_l - v_l - w_l.$$

$G = m_g + n_g e^{-(k2+k6)t} + o_g e^{-(r1+k7)t} + p_g e^{-r2t} + q_g e^{-r3t} + s_g e^{-r4t} + t_g e^{-r5t} + u_g e^{-r6t} + v_g e^{-(k3+r7)t} + w_g e^{-(k8+k9)t} + r_g e^{-(k10+k11)t}$, where

$$m_g = pG3\,\frac{k8 m_e}{(k10 + k11)} \qquad n_g = pG3\,\frac{k8 n_e}{(k10 + k11) - (k2 + k6)}$$

$$o_g = pG3\,\frac{k8 o_e}{(k10 + k11) - (r1 + k7)}$$

$$p_g = pG3\,\frac{k8 p_e}{(k10 + k11) - r2} \qquad q_g = pG3\,\frac{k8 q_e}{(k10 + k11) - r3}$$

$$s_g = pG3\,\frac{k8 s_e}{(k10 + k11) - r4} \qquad t_g = pG3\,\frac{k8 t_e}{(k10 + k11) - r5}$$

$$u_g = pG3\,\frac{k8 u_e}{(k10 + k11) - r6}$$

$$v_g = pG3\,\frac{k8 v_e}{(k10 + k11) - (k3 + r7)}$$

$$w_g = pG3\,\frac{k8 r_e}{(k10 + k11) - (k8 + k9)}$$

$$r_g = G0 - m_g - n_g - o_g - p_g - q_g - s_g - t_g - u_g - v_g - w_g.$$

$I1 = m_{i1} + n_{i1}e^{-(k2+k6)t} + o_{i1}e^{-(r1+k7)t} + p_{i1}e^{-r2t} + q_{i1}e^{-r3t} + s_{i1}e^{-r4t} + t_{i1}e^{-r5t} + u_{i1}e^{-r6t} + v_{i1}e^{-(k3+r7)t} + w_{i1}e^{-(k8+k9)t} + x_{i1}e^{-(k4+r7)t} + y_{i1}e^{-(k4+k8)t} + r_{i1}e^{-k5t}$, where

$$m_{i1} = pG5\,\frac{k4\,m_f}{k5} \qquad n_{i1} = pG5\,\frac{k4\,n_f}{k5-(k2+k6)}$$

$$o_{i1} = pG5\,\frac{k4\,o_f}{k5-(r1+k7)} \qquad p_{i1} = pG5\,\frac{k4\,p_f}{k5-r2}$$

$$q_{i1} = pG5\,\frac{k4\,q_f}{k5-r3} \qquad s_{i1} = pG5\,\frac{k4\,s_f}{k5-r5}$$

$$t_{i1} = pG5\,\frac{k4\,t_f}{k5-r5} \qquad u_{i1} = pG5\,\frac{k4\,u_f}{k5-r6}$$

$$v_{i1} = pG5\,\frac{k4\,v_f}{k5-(k3+r7)} \qquad w_{i1} = pG5\,\frac{k4\,w_f}{k5-(k8+k9)}$$

$$x_{i1} = pG5\,\frac{k4\,x_f}{k5-(k4+r7)} \qquad y_{i1} = pG5\,\frac{k4\,r_f}{k5-(k4+k8)}$$

$$r_{i1} = I10 - m_{i1} - n_{i1} - o_{i1} - p_{i1} - q_{i1} - s_{i1} - t_{i1} - u_{i1} - v_{i1} - w_{i1} - x_{i1} - y_{i1}.$$

$M1 = m_m + n_m e^{-(k2+k6)t} + o_m e^{-(r1+k7)t} + p_m e^{-r2t} + q_m e^{-r3t} + s_m e^{-r4t} + t_m e^{-r5t} + u_m e^{-r6t} + v_m e^{-(k3+r7)t} + w_m e^{-(k8+k9)t} + x_m e^{-(k10+k11)t} + y_m e^{-(k4+r7)t} + z_m e^{-(k4+k8)t} + r_{m1}e^{-(k4+k11)t}$, where

$$m_m = \frac{k10\,m_g + pG3k8\,m_f}{k4+k11} \qquad n_m = \frac{k10\,n_g + pG3k8\,n_f}{k4+k11-(k2+k6)}$$

$$o_m = \frac{k10\,o_g + pG3k8\,o_f}{(k4+k11)-(r1+k7)} \qquad p_m = \frac{k10\,p_g + pG3k8\,p_f}{(k4+k11)-r2}$$

$$q_m = \frac{k10\,q_g + pG3k8\,q_f}{k4+k11-r3} \qquad s_m = \frac{k10\,s_g + pG3k8\,s_f}{k4+k11-r4}$$

$$t_m = \frac{k10\,t_g + pG3k8\,t_f}{k4+k11-r5} \qquad u_m = \frac{k10\,u_g + pG3k8\,u_f}{k4+k11-r6}$$

$$v_m = \frac{k10\,v_g + pG3k8\,v_f}{k4+k11-(k3+r7)} \qquad w_m = \frac{k10\,w_g + pG3k8\,w_f}{(k4+k11)-(k8+k9)}$$

$$x_m = \frac{k10\,r_g}{k4-k10} \qquad y_m = \frac{pG3k8\,x_f}{k11-r7} \qquad z_m = \frac{pG3k8\,r_f}{k11-k8}$$

$$r_m = M0 - m_m - n_m - o_m - p_m - q_m - s_m - t_m - u_m - v_m - w_m - x_m - y_m - z_m.$$

$I2 = m_{i2} + n_{i2}e^{-(k2+k6)t} + o_{i2}e^{-(r1+k7)t} + p_{i2}e^{-r2t} + q_{i2}e^{-r3t} + s_{i2}e^{-r4t} + t_{i2}e^{-r5t} + u_{i2}e^{-r6t} + v_{i2}e^{-(k3+r7)t} + w_{i2}e^{-(k4+r7)t} + x_{i2}e^{-r8t} + r_{i2}e^{-k5t}$, where

$$m_{i2} = \frac{r8\,m_l}{k5} \qquad n_{i2} = \frac{r8\,n_l}{k5-(k2+k6)}$$

$$o_{i2} = \frac{r8\,o_l}{k5-(r1+k7)} \qquad p_{i2} = \frac{r8\,p_l}{k5-r2} \qquad q_{i2} = \frac{r8\,q_l}{k5-r3}$$

$$s_{i2} = \frac{r8\,s_l}{k5-r4} \qquad t_{i2} = \frac{r8\,t_l}{k5-r5} \qquad u_{i2} = \frac{r8\,u_l}{k5-k6}$$

$$v_{i2} = \frac{r8\,v_l}{k5-(k3+r7)} \qquad w_{i2} = \frac{r8\,w_l}{k5-(k4+r7)}$$

$$x_{i2} = \frac{r8\,r_l}{k5-r8}$$

$$r_{i2} = I20 - m_{i2} - n_{i2} - o_{i2} - p_{i2} - q_{i2} - s_{i2} - t_{i2} - u_{i2} - v_{i2} - w_{i2} - x_{i2}.$$